J. Fluid Mech. (1995), *vol.* 287, *pp.* 21–58

Interaction of a potential vortex with a local roughness on a smooth surface

By OLEG S. RYZHOV[1] AND SERGEY V. TIMOFEEV[2]

[1] Department of Mathematical Sciences, Rensselaer Polytechnic Institute, Troy, NY 12180–3590, USA

[2] Computing Center, Russian Academy of Sciences, 40 Vavilov Street, 117333 Moscow, Russian Federation

(Received 23 October 1993 and in revised form 3 October 1994)

Disturbances generated by a potential vortex moving past a small hump or dent on the otherwise smooth flat plate are considered. Features peculiar to this problem derive from the fact that the vortex is stuck with a fixed fluid particle; hence the nonlinear dependence of the pressure on the induced velocity field ensues even if the vortex intensity tends to zero. Formulation of the problem on a flow in the viscous wall sublayer given in canonical variables involves four similarity parameters for any particular shape of a roughness. The parallels between the process at hand and sound scattering from a boundary layer with a small obstacle at the bottom are indicated. Results from numerical integration of the boundary-value problem posed allow us to trace the evolution of the wave-packet structure depending on the potential vortex intensity. Overlapping of the peak wings and formation of an almost continuous spectrum in the Fourier decomposition of the signal serve as a guide for explaining the explosive development of the wave packet as distinct from the Tollmien–Schlichting wavetrain that has been registered experimentally.

The theory developed is applied to discussing the so-called bypass mode of transition provoked by external turbulence. Special emphasis is laid on flows in gas turbine engines where bypass transition plays a dominant role owing to extremely high free-stream turbulence levels.

1. Introduction

The problem of how convected vortices in an effectively inviscid flow interact with the viscous boundary layer on a solid wall has two distinctive aspects primarily depending on the vorticity strength. Up to now, the main efforts from both the theoretical and experimental sides have been concentrated on exploring processes governed by external vortical disturbances of large intensity. Situations of such a kind may arise, for example, in flows past an aircraft wing that are characteristic of take-off and landing conditions. A set-up to simulate these conditions experimentally has been designed by Harvey & Perry (1971). In their observations the trailing vortex shed from the wing tip provoked a boundary-layer separation in the form of a secondary vortex. Walker (1978) was the first to attack the problem on potential vortex/boundary-layer interaction theoretically, in order to elucidate experimental data then available. Firm evidence from observations by Harvey & Perry (1971) and calculations due to Walker (1978) revealed the mechanism for a convected vortex to induce an unsteady boundary-layer separation terminating in the birth of the additional vortex in the vicinity of a solid surface. Very similar situations are typically

observed in rotorcraft flight and gas turbines where the vortical endwall flows trailing each blade impinge against the downstream row of blades. An extensive experimental and computational study of vortex/rotor-blade interactions has been conducted by Caradonna, Strawn & Bridgeman (1988), for a review of gas-turbine-engine flows involving broad discussion of many technical points see Mayle (1991). Another problem where unsteady separation represents one of the dominant features is a pitching airfoil, pertinent data have been summarized by McCroskey (1982). The cause of unsteady separation terminating in the generation of a secondary near-wall vortex is seen in all cases mentioned to be an adverse pressure gradient that was produced by the convected vortex or pitching motion of an airfoil.

The next step has been taken by Doligalski & Walker (1984) in an attempt to explain the bursting phenomena continually occurring in a turbulent boundary layer as the mechanism of vorticity production in the process of a strong viscous/inviscid interaction. Again, the external disturbance was assumed to be a vortex filament convected in a uniform stream past a flat plate, computations being performed for various convection rates of the vortex relative to oncoming flow. The recent applications of this idea in relation to the vorticity regeneration process in flows undergoing transition to turbulence as well as in fully turbulent boundary layers are set forth in Smith *et al.* (1991). Though in a turbulent boundary layer the bursting (eruptive) activity manifests itself through convected hairpin vortices and for this reason is three-dimensional in nature, nevertheless, the process may be approximately viewed as being nearly two-dimensional in the vicinity of the symmetry plane normal to the crescent-shaped ridge of each hairpin vortex.

Thus, in the aforementioned theoretical as well as experimental studies breakdown of a boundary layer owing to formation of a closed bubble with recirculating fluid and ensuing eruption of the rapidly growing eddy is a crucial point determining the essentials of the phenomenon. We are thereby led to the general notion of unsteady separation that is happening under various conditions. The main concern in earlier work on the subject was with the manner in which the boundary layer evolved and thickened. Though at the initiation of the motion the wall shear stress could be positive over the entire body surface, results from both numerical solutions (Collins & Dennis 1973; Cebeci 1979) and asymptotic expansions (Cowley 1983) pointed to the formation of a singularity at some finite instant. Many efforts had been mounted to verify different conjectured structures of the unsteady flow field (see Williams (1977) for an exposition of the so-called Moore–Rott–Sears model) until the complicated nature of the singularity developing under the influence of the prescribed adverse pressure gradient was brought to light by Van Dommelen & Shen (1980). They performed an accurate numerical integration of the classical Prandtl equations in the problem on a circular cylinder impulsively put into motion and revealed boundary-layer focusing into an extremely narrow band at the terminal stage of evolution. This sharp spike involved a vorticity-depleted region which indefinitely shorted in length and thickened in the transverse direction as time approached some particular eruption instant. Van Dommelen & Shen (1982) have also obtained an asymptotic solution describing the singular flow field. When the vorticity-depleted bubble enters the final stage it becomes independent of the pressure distribution in the mainstream. Numerical results presented recently by Peridier, Smith & Walker (1991*a*) for the vortex-induced boundary-layer separation are in excellent agreement with asymptotic focusing of the erupting spike as predicted by the Van Dommelen solution.

It should now be stressed that all analytical and computational studies cited above were performed within the framework of the classical boundary-layer theory by

Prandtl where the pressure gradient is considered to be given in advance from a solution for external potential flow. Therefore the formation of a singularity in the near-wall region might seem to be provoked just by this feature, whereas with viscous/inviscid interaction taken into account the velocity field should retain its smooth behaviour for a longer period of time if the focusing process is not eliminated altogether. Indeed, from its first steps the interacting boundary-layer theory in the form of triple deck put forth in Stewartson (1969), Neiland (1969), Stewartson & Williams (1969), and Messiter (1970) was aimed at ruling out possible discontinuities of different types in viscous shear flows. In line with this methodology, an attempt to mitigate the abrupt focusing of flow into an erupting spike by means of the pressure gradient depending on the induced displacement thickness has been undertaken by Chuang & Conlisk (1989) in their investigations into separation caused by the vortex in motion over a solid surface. However, as has been shown by Brotherton-Ratcliffe & Smith (1987) the complete breakdown of the unsteady velocity field can happen under certain conditions even if the external pressure distribution is to be computed simultaneously with the displacement thickness. The subsequent consideration by Smith (1988) for the general environment testifies to the terminal singularity structure as a generic state that might be reached by most two-dimensional erupting boundary layers at finite time. The existence of the asymptotic structure has been confirmed by recent computations exposed by Peridier *et al.* (1991*b*). Their results show that the role played by interaction in unsteady separation is really twofold: (i) the induced pressure brings an end to the infinite growth of the vorticity-depleted zone towards the upper reaches of the boundary layer, implying that the eruptive process becomes less acutely pronounced, (ii) on the other hand, occurrence of the singular behaviour in the instantaneous streamline pattern is accelerated being accompanied by bifurcation of the secondary eddy into several smaller bubbles with reversed flow.

Completely different features are inherent in the disturbance pattern when the strength of a potential vortex is fairly weak and it moves at a comparatively small distance from the solid surface. In this case, the vortex does not violate the boundary-layer structure to leading order, on the contrary, the response of the viscous near-wall region to the vortex motion is passive, no separation starts to develop in this thin so-called Stokes sublayer. Therefore the classical approach due to Prandtl is applicable in full measure for describing smooth external and internal velocity fields in a regular manner. Some rough elements should be included into the body contour for the viscous/inviscid interaction process to become operative. Thus, we are naturally led to a problem of the boundary-layer receptivity aimed at clarifying the issue of how fairly weak disturbances that can vary in physical nature penetrate into the boundary layer and are transformed into Tollmien–Schlichting eigenmodes. In general terms, the problem has been posed by Morkovin (1969), for recent progress towards understanding this complicated phenomenon see Goldstein & Hultgren (1989), Kerschen (1989), and Kozlov & Ryzhov (1990) and references therein.

The receptivity mechanism in question was briefly outlined in Ryzhov (1989) and Kozlov & Ryzhov (1990) in view of some features peculiar to it. First, insofar as the vortex is stuck with a fixed fluid particle the nonlinear dependence of the pressure on the induced velocity field ensues in the potential flow region even if the vortex strength tends to zero. Secondly, the interaction between the travelling vortex and local variations in surface geometry is essentially nonlinear and stems from quadratic terms entering the unsteady boundary-layer equations. When confining to the weak vortical intensities one may linearize the original system of equations; the linear approximation falls into two parts owing to the superposition principal. The steady term accounts for

changes produced in the oncoming shear flow by the roughness, whereas the time-dependent part of the linear solution is given by relations coming from the Stokes sublayer. This second part may be calibrated so as to provide time-scale coupling between the external disturbance and Tollmien–Schlichting eigenmodes through making an appropriate choice of the vortex strength and location, but under such conditions the streamwise spatial scale turns out to be of order of the convective reference length. In the limit as the Reynolds number tends to infinity, the ratio of the wavelengths of unstable Tollmien–Schlichting eigenmodes to the reference length of the free-stream vortical disturbances becomes very small. On the other hand, the streamwise spatial scale required for matching with viscous eigenmodes may be introduced into the problem by means of inhomogeneities in the steady velocity field owing to variations in the solid-body geometry. Obviously, the quadratic terms are to be taken into consideration for describing the interaction. In the next approximation the system of governing equations is also linear but inhomogeneous, contributions to the right-hand sides of these equations being given by the products of both parts of the linear solutions. So, just allowing for the quadratic terms creates a mechanism to excite the Tollmien–Schlichting eigenmodes. According to Ruban (1984) and Goldstein (1985), a similar mechanism underlies the scattering of harmonic acoustic signals into unstable oscillations in the boundary layer by a small hump or dent on an otherwise flat plate. The scattering process is extremely sensitive even with respect to a sudden change in the surface curvature (Goldstein & Hultgren 1987).

Another feature to be pointed out with regard to the potential vortex/small roughness interaction is the emission of a wave packet (vortex spot) instead of an isolated monochromatic wavetrain that predominantly finds use in wind-tunnel tests. The structure of the wave packet is primarily determined by pulsations with the largest amplitude growth rate, this maximum being located in the vicinity of the lower branch of the neutral stability curve in the limit of high Reynolds numbers (Zhuk & Ryzhov 1983). Hence, it is clear, and results of calculations corroborate, that at the linear stage of development the wave packets excited by any external agency operating in the pulse mode are practically identical. However, disturbances of this type bear some distinctive properties since they incorporate wave modulation from the site of birth. As Gaster (1975) first highlighted, owing to vitally important modal interaction, the wave-packet propagation happens explosively, growing pulsations enter the nonlinear stage very rapidly, and then break down giving rise to a turbulent spot. However, computations in this pioneering work were in point of fact based on unvalidated assumptions. Careful asymptotic analysis subsequently performed by Ryzhov & Terent'ev (1984, 1986) within the framework of linearized two-dimensional triple-deck theory has lent credence to the standpoint of Gaster (1975) that the violent nature was characteristic of vortical wave-pulse amplification. Extension of the linear asymptotic analysis in Ryzhov & Savenkov (1987) gave solid grounds for three-dimensional wave-packet calculations using the steepest descent approach and revealed a resemblance of the two-dimensional and three-dimensional pulsation structures. Analogous results were set forth in Duck (1987). A conclusion of principal importance to be drawn from all these studies points to extremely dissimilar behaviour of the harmonic wavetrains and modulated wave packets: disturbances of the first type gain strength gradually with distance, unlike travelling and spreading oscillations of the second type which may be viewed as blowing up in time and space. According to Ryzhov & Savenkov (1989, 1991) and Smith (1991), vigorous development of the wave packet also persists in the nonlinear regime, preventing numerical procedures applied to the interacting boundary-layer equations from being continued beyond a certain stage where strong

irregularities in the signal shape appear and grow steeply. Experimental verification of the violent nature of the modulated signal propagation has been provided by Gaster & Grant (1975); in their quiet wind-tunnel tests, wave packets were created by introducing weak impulse-like puffs through a small hole in a flat plate and registered up to the onset of the nonlinear distortions appearing in the central cycles of pulsations. Later on Gaster (1980, 1981) continued his observations on artificially generated vortex spots to enable the conditions of their breakdown to occur in a controlled manner. Recently, an extensive study on the evolution of a weak localized disturbance was conducted by Breuer & Haritonidis (1990), subsequent results pertaining to a strong disturbance was reported in Breuer & Lanfahl (1990). The development of localized disturbances in a boundary layer from the small-amplitude wave-packet stage up to the ultimate formation of a turbulent spot has been traced in low-turbulence wind-tunnel tests by Cohen, Breuer & Haritonidis (1991), with the main focus on nonlinear effects. In keeping with the aforesaid, experimental data are indicative of great distinctions in the routes to transition peculiar to monochromatic wavetrains and modulated wave packets.

The first attempt to inquire into the essentially nonlinear interaction induced by a strong convected vortex filament on the boundary layer over a flat plate with a small hump has been undertaken in the work by Chuang & Conlisk (1989) cited above. As they claimed, depending on the vortex strength, the calculations might be continued significantly beyond the non-interactive flow regime considered by Doligalski & Walker (1984). However, the main result was the observation of a small tertiary eddy formed in the latest phase of computations. It follows from the foregoing discussion of the work by Peridier *et al.* (1991*b*) that this additional eddy must eventually terminate in the singular focusing of the interacting boundary layer asymptotically described by solutions from Brotherton-Ratcliffe & Smith (1987) and Smith (1988). Apparently for this reason, the excitation of the Tollmien–Schlichting eigenmodes in the form of a modulated wave packet was not detected in the essentially nonlinear vortex/hump interaction process. The situation parallels to some extent that in another nonlinear receptivity problem on a large-amplitude vibrator installed on an otherwise flat surface where Duck (1985, 1987) found an extremely irregular disturbance pattern shortly after the beginning of generation. Unstable inviscid Rayleigh eigenmodes for the basic velocity profile were computed by Duck (1988) with reference to some correlation between the magnitude of their growth rate and the occurrence of the apparent singularity, leading to the breakdown of a numerical solution. Recently, a quite different approach has been proposed (Bodonyi *et al.* 1989) if only to partially overcome difficulties in computational studies. The steady flow was taken to be of the viscous–inviscid nonlinear interactive type while the unsteady disturbances were assumed to be governed by the Navier–Stokes equations linearized about this flow.

The focus in the present work is in the computational study of the vortex–filament/local roughness interaction provided that the process be considered mild in the terms used in the above discussion. On this assumption, interaction terminates in the emission of a wave packet rather than in the focusing of a boundary layer into a narrow band. So, in the regime to be analysed below, Tollmien–Schlichting instabilities comes into play first thereby preventing an eddy of recirculating fluid from being formed and growing to appreciable sizes.

A schematic diagram of the vortex/roughness interaction showing regions with asymptotically different properties is presented in figure 1. A small parameter ϵ inherent in the triple-deck theory is introduced through the Reynolds number R_L as $\epsilon = R_L^{-1/8}$ (an exact definition of the Reynolds number will be given in §2). Three tiers,

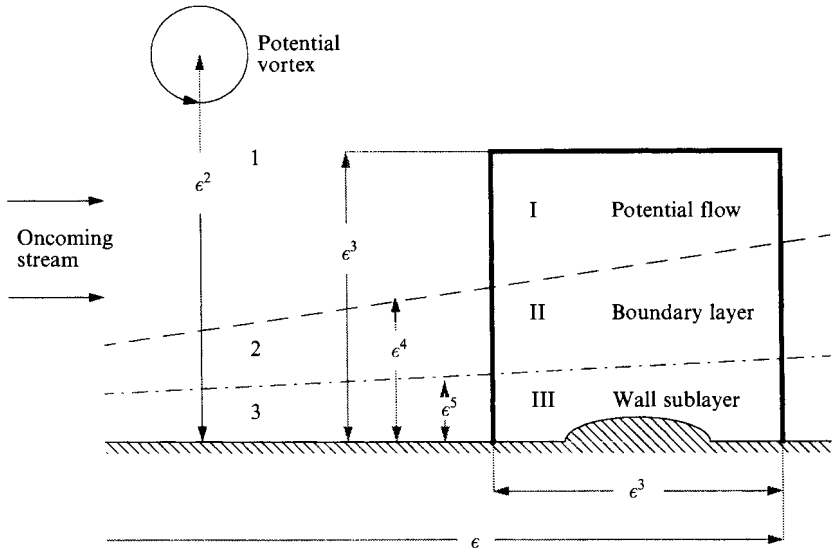

FIGURE 1. Schematic diagram (not to scale) of the potential convected vortex/surface-roughness interaction. In a long non-interaction region which extends upstream and consists of three tiers 1, 2, 3 disturbances are driven by the vortex-induced pressure gradient. The region centred around a local hump (or dent) involves three decks I, II, III where the strong viscous/inviscid interaction determines for the most part variations of the pressure.

1, 2 and 3, are used to specify the flow field at long distances upstream of a hump or dent. Most of the boundary layer 2 and the Stokes sublayer 3 at its bottom, whose length is proportional to ϵ, are passive and driven by the pressure gradient induced by the convected vortex in the nearly uniform potential stream 1. Solutions here are independent of the interaction process downstream. The vortex elevation of order ϵ^2 above the solid surface is chosen so as to produce disturbances in the region of viscous/inviscid interaction around the plate imperfection which are scaled as suggested by the triple-deck approach, the vortex strength being determined from analogous considerations. The interaction region consists also of three tiers I, II and III of the same length proportional to ϵ^3. So, the effective longitudinal scale of order ϵ^2 intrinsic to the vortex filament is intermediate between the reference lengths of the two distinct regions mentioned above. Disturbances in the near-wall sublayer III evolve under the influence of the self-induced pressure created in potential flow I and transmitted across the main part of boundary layer II in a passive way. However, initial distributions of fluid parameters far upstream of the obstacle in each of these decks derive from the matching with known solutions for the Stokes sublayer 3, nearly uniform stream 1 and most of the boundary layer 2, respectively. Besides, the latter solutions contribute to matching conditions to be posed for all three decks within the region where viscous/inviscid interaction takes place.

In §2 the external potential field is expressed in scaled variables using the small parameter ϵ to ensure the triple-deck formalism which will later on be applicable to nonlinear calculations of the boundary-layer receptivity. The flow pattern in most of the boundary layer over a flat plate analysed in §3 exhibits some specific features due to vortex motion at the velocity of a fluid particle, as a consequence singularity enters asymptotic expansions when approaching the upper reaches of this region. As shown in §4 in accord with what has been said, the viscous wall sublayer behaves in a manner typical of a passive Stokes layer, no erupting spikes develop here since the vortex

strength is weak. This brings an end to developing solutions under the action of the known pressure gradient induced by the convected potential vortex. Sections 5–7 describe the interaction stage in the vicinity of a small hump or dent located on the plate, a boundary-value problem for the viscous wall sublayer involves time-dependent terms arising from the vortex-induced pressure and velocities. The boundary-value problem is reformulated in canonical variables in §8 to reduce the number of similarity parameters to four provided that the shape of the roughness is fixed. The parallels between the process at hand and sound scattering from a boundary layer with a local surface imperfection at the bottom are indicated in §9. Results of computations are presented in §10, they point to wave-packet generation when the vortex passes over an obstacle, the oscillation amplitude (of order 1 in scaled variables) being determined by the obstacle sizes. The receptivity mechanism is essentially the same as in the linear problem in spite of it being governed by the full system of Prandtl equations with the self-induced pressure gradient coming from interaction. The wave packets nonlinearly emitted evolve explosively in all calculations, revealing in the wall-shear-stress distributions very short wavelets which distort the positive phases of each oscillation cycle. The negative phases turn out to be narrower and more intensive, they are not susceptible to large distortions on the short lengthscale. In order to explain vigorous development of the wave packets their Fourier decompositions are plotted as functions of the wavenumber. Overlapping of the peak wings and formation of an almost continuous spectrum for these modulated signals are apparently responsible for their blow-up. Similar results derive from sound-scattering computations briefly presented in §11. Concluding remarks in §12 are primarily aimed at the application of the theory developed for elucidating the bypass mode of transition in gas-turbine-engine flows.

2. A vortex in a uniform incompressible stream

Let us consider a vortex that is carried along by a uniform incompressible stream of velocity U_∞^* past a flat plate with a small imperfection in its shape. More precisely, we assume that a local roughness in the form of a hump or dent is located on the solid surface and submerged into the boundary layer (see figure 1). The problem is to study the vortex passage over the obstacle and the interaction process with inhomogeneities in the pressure and velocity fields provoked by this obstacle. Our main concern will be with a wave packet generated in the boundary layer. Results based on a linear analysis point to the excitation of unstable modulated oscillations in a thin near-wall region of the flow (Ryzhov 1989; Koslov & Ryzhov 1990). On the other hand, Chuang & Conlisk (1989) have not revealed in their nonlinear calculations any wave packet to arise from interaction.

A starting point of what follows is the potential function

$$\phi^* = U_\infty^* L^* \Delta \tan^{-1} \frac{x^* - L^*}{y^* - l^*} \tag{2.1}$$

of a rectilinear vortex filament in incompressible fluid which occupies an unbounded space and is at rest at infinity. Here x^*, y^* are Cartesian coordinates; two constants l^* and L^* fix the location of the vortex with respect to the solid surface; Δ introduces a normalization multiplier.

Two points need to be taken into account. First, the effect of a flat plate results in a solution for the potential flow region in the form of a pair of counter-rotating vortices

that are symmetric about the solid surface at every instant. This superposition holds provided that the separation $2l^*$ between the vortices is much less than the distance L^* from the leading edge of the plate to a straight line connecting both vortices. As is well known (Milne-Thompson 1962), the vortex pair does not remain at rest in a quiescent fluid, on the contrary it moves along the symmetry line $y^* = 0$ with velocity $c_v^* = U_\infty^* L^* \Delta/(2l^*)$. Secondly, it is necessary to bear in mind that the flat plate is submerged into a uniform stream whose velocity is U_∞^* in the absence of vortices. From this it follows that the velocity c^* of the vortex-pair motion in the laboratory frame of reference is $c^* = U_\infty^*[1 + L^*\Delta/(2l^*)]$. The same model was originally proposed by Walker (1978) and Doligalski & Walker (1984) in calculations of the boundary layer induced on a flat plate by a two-dimensional vortex, the final stage of the strong erupting process terminating in the focusing of the boundary layer into a very narrow bands was described in Peridier *et al.* (1991*a*, *b*).

Unlike the papers cited, the further analysis of fluid oscillations occurring in the viscous flow region is performed here within the framework of the asymptotic triple-deck theory due to Stewartson (1969), Neiland (1969), Stewartson & Williams (1969), and Messiter (1970) as applied to an interacting boundary layer with the self-induced pressure gradient. The theory starts from introducing a small parameter $\epsilon = R_L^{-1/8}$ with the Reynolds number R_L being assumed to tend to infinity. In accordance with basic concepts adopted in the triple deck we suppose the non-dimensional time to be of order ϵ^2. Insofar as $x^* - L^* = O(U_\infty^* t^*)$ where t^* is the time measured in initial dimensional units, the non-dimensional local distance along the x^*-axis is also estimated by ϵ^2. In the potential velocity field labelled 1 in figure 1 both directions are to be treated equally, therefore the non-dimensional distance along the y^*-axis is likewise of order ϵ^2. Thus, we may put

$$t^* = \epsilon^2 \frac{L^*}{U_\infty^*} t', \quad x^* = L^*(1 + \epsilon^2 x'), \quad y^* = \epsilon^2 L^* y_1', \quad l^* = \epsilon^2 L^* b_0. \quad (2.2a\text{–}d)$$

An expression for the potential function ensues from (2.1) with allowance made for the above remarks, it should be written in scaled variables as well. The proper choice of Δ turns out to be non-trivial to some extent because a relation between the pressure and velocity field induced by a vortex is nonlinear. In order to deal with disturbances of order ϵ in the near-wall Stokes sublayer (see §4), that provide a match with the viscous/inviscid interaction region centred around an obstacle downstream, we need to put $\Delta = O(\epsilon^{5/2})$. With the final scaling $\Delta = \epsilon^{5/2}\delta_0$, $\delta_0 = O(1)$ of the normalization multiplier we get

$$\phi^* = U_\infty^*[x^* + \epsilon^{5/2} L^* \phi_1'(t', x', y_1')], \quad (2.3a)$$

$$\phi_1' = \delta_0 \left(-\tan^{-1} \frac{x' - ct'}{y_1' - b_0} + \tan^{-1} \frac{x' - ct'}{y_1' + b_0} \right), \quad (2.3b)$$

where $c = c^*/U_\infty^* = 1 + c_v$ and $c_v = c_v^*/U_\infty^* = \epsilon^{1/2}\delta_0/(2b_0)$ defines the intrinsic velocity of vortices. Velocity components corresponding to (2.3*a*, *b*) are

$$u^* = U_\infty^*[1 + \epsilon^{1/2} u_1'(t', x', y_1')], \quad v^* = \epsilon^{1/2} U_\infty^* v_1'(t', x', y_1'), \quad (2.4a, b)$$

$$u' = \delta_0 \left[-\frac{y_1' - b_0}{(x' - ct')^2 + (y_1' - b_0)^2} + \frac{y_1' + b_0}{(x' - ct')^2 + (y_1' + b_0)^2} \right], \quad (2.4c)$$

$$v' = \delta_0 \left[\frac{x' - ct'}{(x' - ct')^2 + (y_1' - b_0)^2} - \frac{x' - ct'}{(x' - ct')^2 + (y_1' + b_0)^2} \right], \quad (2.4d)$$

whence it follows that

$$u_1' = \delta_0 \frac{2b_0}{(x'-ct')^2+b_0^2}, \tag{2.5}$$

at the symmetry axis $y_1' = 0$. All that remains to be done is to evaluate the difference between the local pressure p^* and its unperturbed value p_∞^* in an oncoming stream. For a fluid of density ρ^*, substituting (2.4*a*), (2.5) into the Lagrange–Cauchy integral yields

$$p^*-p_\infty^* = \epsilon\rho^* U_\infty^{*2} p_1'(t', x', y_1'), \tag{2.6a}$$

$$p_1'(t', x', 0) = -\tfrac{1}{2}\delta_0^2\left\{\left[-\frac{1}{2b_0}+\frac{2b_0}{(x'-ct')^2+b_0^2}\right]^2-\left(\frac{1}{2b_0}\right)^2\right\}. \tag{2.6b}$$

It is worthy of notice that variations of the non-dimensional velocities and pressure are of a different order in magnitude, for they are connected through a nonlinear dependence, as mentioned above.

A similar problem on the vortex/boundary-layer interaction has been considered by Doligalski & Walker (1984) for different values of the fractional convection rate

$$\alpha = c = c^*/U_\infty^* = 1+\epsilon^{1/2}\delta_0/(2b_0). \tag{2.7}$$

Although the mathematical formulation of the problem in their work was different from what follows, it is instructive to point out a conclusion of basic importance to be drawn from calculated results. If $\alpha < 0.75$, a rapid lift-up of the boundary-layer streamlines accompanied by strong boundary-layer growth occurs in the region behind the vortex. In the final stage the process terminates in a separation phenomenon in the form of the secondary eddy and its spike-like bursting. As α increases, the relative width of the boundary-layer eddy diminishes and the region of strong boundary-layer growth narrows. On the other hand, if $\alpha > 0.75$ the flow evolution within the boundary layer is more gradual, the integrations could be carried out to larger times without revealing separation with the secondary eddy. The existence of the threshold value $\alpha = 0.75$ is easily derivable from the properties of the velocity field (2.4*a–d*) induced by the original potential vortex. For $\alpha < 0.75$, the effects of the vortex are strong enough to create a region with recirculating fluid bounded by two stagnation points located on the wall below the vortex. In the limit case $\alpha = 0.75$, the two stagnation points merge directly beneath the moving vortex and no flow reversal occurs here. For $\alpha > 0.75$, the flow near the solid surface is retarded under the vortex but is always in the direction of the oncoming stream. Hence it follows that weak vortices convected close to the wall as $\alpha \to 1$ call, in view of $\epsilon \to 0$ in (2.7), for a special treatment because viscous instabilities may manifest themselves in full measure prior to the developing of separation bursting which is delayed to a later stage. However, in view of (2.4*a*, *b*) characteristic values of both induced velocity components are proportional to $R_L^{-1/16}$, as for the gradients of these components and pressure, they are as large as $O(R_L^{3/16})$ and $O(R_L^{1/8})$, respectively. So, in practical terms the vortex intensity is not very weak.

3. Boundary layer

Let us turn to most of the boundary layer over a smooth part of a plate upstream of a local roughness. Here the transverse coordinate is $y^* = \epsilon^4 L^* y_2$. Confining ourselves to a region of fairly small extent in the longitudinal direction the length of which is estimated for instance through $x^* = L^*(1+\epsilon x_1')$, we may suppose the fluid

velocity in the initial unperturbed motion to be dependent on y_2 only. Then the first terms of asymptotic sequences for desired functions are written down as

$$u^* = U_\infty^* u_2' = U_\infty^* [u_{20}(y_2) + \epsilon u_{21}'(x_1', y_2)\, U(X) + \ldots], \tag{3.1a}$$

$$v^* = U_\infty^* v_2' = U_\infty^* [\epsilon^3 v_{21}'(x_1', y_2)\, V(X) + \ldots], \tag{3.1b}$$

$$p^* = p_\infty^* + \rho^* U_\infty^{*2} [\epsilon p_{21}'(x_1', y_2)\, P(X) + \ldots], \tag{3.1c}$$

with an obvious definition $X = x' - ct'$ of the short-scaled variable that is inherent in the inner structure of the potential vortex convected above the flat plate. As for the function u_{20}, it gives the velocity profile in the region of the Blasius boundary layer under examination.

Substituting (3.1*a–c*) into the original Navier–Stokes equations yields

$$P = U, \quad V = \frac{\mathrm{d}U}{\mathrm{d}X}, \tag{3.2a, b}$$

and in addition

$$u_{21}' + \frac{\partial v_{21}'}{\partial y_2} = 0, \quad u_{21}'(u_{20} - c) + v_{21}' \frac{\mathrm{d}u_{20}}{\mathrm{d}y_2} = -p_{21}', \quad \frac{\partial p_{21}'}{\partial y_2} = 0. \tag{3.3a–c}$$

From (3.3*c*) we conclude that $p_{21}' = p_{21}'(x_1')$. A solution to (3.3*a*, *b*), satisfying the slip condition $v_{21}' = 0$ at $y_2 = 0$, reads

$$u_{21}' = -\frac{p_{21}'}{u_{20} - c} - \frac{\mathrm{d}u_{20}}{\mathrm{d}y_2} \int_0^{y_2} \frac{p_{21}'}{(u_{20} - c)^2} \mathrm{d}y_2, \tag{3.4a}$$

$$v_{21}' = (u_{20} - c) \int_0^{y_2} \frac{p_{21}'}{(u_{20} - c)^2} \mathrm{d}y_2. \tag{3.4b}$$

Since $\mathrm{d}u_{20}/\mathrm{d}y_2$ decays exponentially fast at the outer reaches of the boundary layer, the asymptotic behaviour of the velocity field, as $y_2 \to \infty$, is to leading order fixed by

$$u_{21}' \to \epsilon^{-1/2} p_{21}' \left(\frac{\delta_0}{2b_0}\right)^{-1}, \quad v_{21}' \to -\epsilon^{-1/2} p_{21}' \left(\frac{\delta_0}{2b_0}\right)^{-1} y_2.$$

The estimates obtained conform with the velocity components' scaling, adopted in (2.4*a*, *b*) for the potential flow region to within an order of the same power of ϵ but differ in functional dependence on t', x' and x_1'. Hence it follows that both relations (3.4*a*, *b*) are not uniformly valid in most of the boundary layer. Strictly speaking, the region where $|u_{20}(y_2) - 1| = O(\epsilon^{1/2})$ must be considered as an additional sublayer to be analysed separately. The direct matching of the potential velocity field (2.4*a*, *d*) with expansions (3.1*a*, *b*) for the boundary layer is impossible without special analysis.

In order to get around the difficulty, we take advantage of the fact that the pressure does not vary along the transverse coordinate. Insofar as the expression for the pressure remains regular when approaching the outer edge of the boundary layer, in spite of singularities entering the velocity field, the functions on the right-hand side of (3.1*c*) are $p_{21}' = 1$, $P = p_1'(t', x', 0)$, the latter being given by (2.6*b*). Let us go over now into a moving frame of reference that is stuck with the potential vortex above the flat plate; the velocity components here are designated by means of u_s^*, v_s^*. In the approximation under discussion, u_{20} is assumed to be a function of y_2 only,

consequently the flow within the boundary layer proves to be steady and obeys obvious conditions

$$u_s^* = U_\infty^* u'_{s2} = U_\infty^* [u_{20}(y_2) - c], \quad v_s^* = U_\infty^* v'_{s2} = 0, \tag{3.5a, b}$$

at infinity. A relationship between the non-dimensional velocities u'_{s2}, v'_{s2} and the pressure $p'_2 = P(X) = p'_1(t', x', 0)$ along every streamline $\psi_2 = \text{constant}$, is fixed by the Bernoulli integral

$$\tfrac{1}{2}(u'^2_{s2} + v'^2_{s2}) + \epsilon p'_2 = h(\psi_2) = \tfrac{1}{2}[u_{20}(y_2) - c]^2. \tag{3.6}$$

To arrive at a final form of h, we need to express the transverse coordinate y_2 in terms of ψ_2 making use of the relation

$$\psi_2 = \int_0^{y_2} [u_{20}(\sigma) - c]\, \mathrm{d}\sigma$$

ensuing from (3.5*a*, *b*). It follows herefrom that $\psi_2 \to -y_2$ as $y_2 \to 0$, whereas $\psi_2 \to \psi_{20} - c_v y_2$ with a constant

$$\psi_{20} = \int_0^{\infty} [u_{20}(\sigma) - 1]\, \mathrm{d}\sigma, \tag{3.7}$$

if $y_2 \to \infty$. For y_{20} tends to 1 exponentially fast as $y_2 \to \infty$, converges of an improper integral on the right-hand side of (3.7) is assured.

Let us show that the longitudinal velocity u'_{s2} evaluated from the Bernoulli integral meets a condition that provides matching with the external potential flow. As $\psi_2 \to \psi_{20} - c_v y_2, y_2 \to \infty$, the asymptotics of (3.6) reads

$$u'_{s2} \to \epsilon^{1/2} \delta_0 \left(-\frac{1}{2b_0} + \frac{2b_0}{X^2 + b_0^2} \right). \tag{3.8}$$

On the other hand, an obvious expression

$$u'_2 \to 1 + \epsilon^{1/2} u'_1(t', x', 0) \quad \text{as} \quad y_2 \to 0$$

may be written relying on (2.4*a*). Taking into account a relation $u_s^* = u^* - (U_\infty^* + c_v^*)$ between longitudinal velocity components in the laboratory and moving frames of reference we come to recognize that the latter expression does coincide with (3.8) on the strength of (2.5) for $u'_1(t', x', 0)$.

Besides, a limit value of u'_{s2} as $\psi_2 \to -y_2, y_2 \to 0$ is to be indicated. In this case the Bernoulli integral yields

$$u'_{s2} \to -1 + \frac{\mathrm{d}u_{20}(0)}{\mathrm{d}y_2} y_2 - \epsilon^{1/2} \delta_0 \frac{1}{2b_0} - \tfrac{1}{2}\epsilon \delta_0^2 \left[\left(-\frac{1}{2b_0} + \frac{2b_0}{X^2 + b_0^2} \right)^2 - \left(\frac{1}{2b_0} \right)^2 \right]. \tag{3.9}$$

An analogous limit for the longitudinal velocity in the frame of reference at rest can be determined on the basis of (3.1*a*). As (3.4*a*) suggests, $u'_{21} \to 1$ as $y_2 \to 0$ if the correction term $c_v = \epsilon^{1/2}\delta_0/(2b_0)$ in the fractional convection rate $\alpha = c = 1 + 1c_v$ is disregarded as compared to 1. Hence, we have the desired limit in the form

$$u'_{21} \to \frac{\mathrm{d}u_{20}(0)}{\mathrm{d}y_2} y_2 + \epsilon U(X), \tag{3.10}$$

which easily reduces to (3.9) by means of (3.2*a*). Thus, the solution (3.4*a*, *b*) in question is applicable for describing most of the boundary layer except for a region with $|u_{20}(y_2) - 1| = O(\epsilon^{1/2})$ located towards its upper edge.

4. Stokes layer

In the viscous near-wall sublayer 3 of figure 1, the desired functions are expanded in asymptotic sequences

$$u^* = U_\infty^* [\epsilon u'_{30}(t', x', y_3) + \ldots], \tag{4.1a}$$

$$v^* = U_\infty^* [\epsilon^4 v'_{30}(t', x', y_3) + \ldots], \tag{4.1b}$$

$$p^* = p_\infty^* + \rho^* U_\infty^{*2} [\epsilon p'_{31}(t', x', y_3) + \ldots], \tag{4.1c}$$

where the transverse coordinate is scaled through $y^* = \epsilon^5 L^* y_3$ in accordance with the triple-deck theory by Stewartson (1969), Neiland (1969), Stewartson & Williams (1969) and Messiter (1970). The system of governing equations is written down as

$$\frac{\partial u'_{30}}{\partial x'} + \frac{\partial v'_{30}}{\partial y_3} = 0, \quad \frac{\partial u'_{30}}{\partial t'} = -\frac{\partial p'_{31}}{\partial x'} + \frac{\partial^2 u'_{30}}{\partial y_3^2}, \quad \frac{\partial p'_{31}}{\partial y_3} = 0. \tag{4.2a–c}$$

The function $p'_{31} = P(X) = p'_1(t', x', 0)$ is an evident solution to (4.2c). As a result, (4.2b) separates from other equations to give

$$\frac{\partial u'_{30}}{\partial t'} = -\frac{\mathrm{d}P}{\mathrm{d}X} + \frac{\partial^2 u'_{30}}{\partial y_3^2}. \tag{4.3}$$

The transverse velocity component v'_{30} is evaluated from (4.2a) upon computing the longitudinal velocity u'_{30} from (4.3). The boundary condition for u'_{30} at the upper reaches of the Stokes layer is obtainable from the matching of (4.1a) with (3.1a) and (3.10), namely

$$u'_{30} - \frac{\mathrm{d}u_{20}(0)}{\mathrm{d}y_2} y_3 \to P(X) \quad \text{as} \quad y_3 \to \infty. \tag{4.4}$$

At the flat plate $y_3 = 0$ we have to meet the no-slip condition $u'_{30} = 0$. A comment concerning the short-scaled variable $X = x' - ct'$ is pertinent at this point. Taking into account the correction term $c_v = \epsilon^{1/2}\delta_0/(2b_0)$ plays an essential part only when approaching the upper edge of the boundary layer. As for the viscous near-wall sublayer, this term should be omitted, just as it has been disregarded in deriving the limit (3.10). Therefore we may put

$$X = x' - t', \tag{4.5}$$

in analysis of both the Stokes layer and near-wall sublayer in a region of strong viscous/inviscid interaction which extends farther downstream.

With allowance made for (4.5), a particular solution of the non-homogeneous equation (4.3) is $u'_{30} = P(X)$. Representing the desired solution in the form

$$u'_{30} = \frac{\mathrm{d}u_{20}(0)}{\mathrm{d}y_2} y_3 + P(X) + U'_{30}(t', x', y_3), \tag{4.6}$$

we arrive at the conclusion that the function U'_{30} satisfies the homogeneous heat-conduction equation in t' and y_3. As $y_3 \to \infty$, a homogeneous limit condition $U'_{30} \to 0$ ensues from (4.4), whereas a non-homogeneous boundary condition $U'_{30} = -P(X)$ holds at the plate $y_3 = 0$. A feature peculiar to the boundary-value problem posed lies in absence of initial data. Its solution,

$$U'_{30} = -\frac{1}{2\pi^{1/2}} \int_{-\infty}^{t'} \frac{y_3}{(t'-\tau)^{3/2}} \exp\left[-\frac{y_3^2}{4(t'-\tau)}\right] P(x'-\tau)\,\mathrm{d}\tau, \tag{4.7}$$

completes the analysis of disturbances developing in the boundary layer under the action of a given pressure gradient induced by a potential vortex in motion.

So, the Stokes sublayer responds to the motion of a potential vortex in a passive manner if its strength becomes small enough. The Reynolds number R_l introduced in Doligalski & Walker (1984) is based on the distance l^* separating the vortex from the wall, hence $R_l = \epsilon^2 R_L$. The vortex-induced velocities on the right-hand side of (2.4*a*, *b*) may be thought of as being expressed in terms of $\epsilon = R_l^{-1/6}$ rather than $\epsilon = R_L^{-1/8}$. Both scaled components u' and v' given by (2.4*c*) and (2.4*d*), respectively, remain the same when the definition of ϵ changes. Generation of growing disturbances by the weak potential vortex can occur in the process of its interaction with a small roughness located at the bottom of a boundary layer. However, Tollmien–Schlichting waves have not been seen in calculations by Chuang & Conlisk (1989) of the vortex in motion over a hump. A plausible explanation for their results lies in conditions which were chosen to be similar to those in Doligalski & Walker (1984), and is twofold. First, the length of the obstacle was of order l^* and therefore too large for Tollmien–Schlichting eigenmodes of sufficient amplitude to be excited and become really operative on their intrinsic timescale. Secondly, the vortex intensity was fairly strong for a small tertiary eddy to arise and then terminate in the singular focusing during the interactive phase. In order to reveal the wave-packet emission in the process of viscous/inviscid interaction, we need to consider humps or dents on an otherwise flat plate which are shorter by an order of magnitude, that is to say, their length must be $O(\epsilon l^*)$. This assumption is at the heart of the following analysis.

5. Potential region in the vortex/roughness interaction

According to the aforementioned statement, the sizes of this region labelled I in figure 1 are to be scaled through

$$x^* = L^*(1+\epsilon^3 x_i), \quad y^* = \epsilon^3 L^* y_{1i}, \tag{5.1a, b}$$

whereas the non-dimensional time is defined by (2.2*a*). It follows that conditions for desired fluid parameters to be matched to analogous parameters of the potential vortex over a smooth part of a plate must be imposed as $x' \to 0$, $x_i \to -\infty$ and $y_1' \to 0$, $y_{1i} \to \infty$. A limit expression ensuing from (2.6*a*) shows that the excess pressure is expanded in an asymptotic sequence of the form

$$p^* - p_\infty^* = \rho^* U_\infty^{*2}[\epsilon p_{11}(t') + \epsilon^2 p_{12}(t', x_i, y_{1i}) + \ldots]. \tag{5.2}$$

Here the leading term $p_{11} = p_1'(t', 0, 0)$ to be obtained with the help of (2.6*b*) reads

$$p_{11} = -\tfrac{1}{2}\delta_0^2\left[\left(-\frac{1}{2b_0} + \frac{2b_0}{(ct')^2 + b_0^2}\right)^2\right] - \left(\frac{1}{2b_0}\right)^2. \tag{5.3}$$

As for the correction term p_{12}, the flow pattern in the two lower decks depends only on its limit value

$$p_{12}(t', x_i, 0) \to -\delta_0^2 \frac{4b_0 t'}{(t'^2 + b_0^2)^2}\left(-\frac{1}{2b_0} + \frac{2b_0}{t'^2 + b_0^2}\right) x_i \quad \text{as} \quad x_i \to \infty. \tag{5.4}$$

We may also write down the corresponding asymptotic representation of the velocity field and inquire into its properties in the limit as $x_i \to -\infty$, $y_{1i} \to \infty$ that is of primary concern for matching. The leading term of order $\epsilon^{1/2}$ in the expression for the perturbed longitudinal component is, in view of (2.4*a*, *c*), a function of t'. The next term of order

$\epsilon^{3/2}$ features linear behaviour both in x_i and y_{1i} when approaching the limit in question. An expansion for the transverse velocity component begins with a term of order $\epsilon^{3/2}$ which is proportional to y_{1i} at infinity. As can be seen from (2.4*b*, *d*), a term of order ϵ^2 makes no contribution to be quadratic in x_i and y_{1i} in the limit as $x_i \to -\infty$, $y_{1i} \to \infty$. The quadratic form in x_i and y_{1i} first arises in this limit owing to the contribution from a term of order $\epsilon^{5/2}$. We may conclude that the problem on a function p_{12} entering the right-hand side of (5.2) is reducible to the Laplace equation in x_i and y_{1i}. The latter is characteristic of the free interaction theory developed in Stewartson (1969), Neiland (1969), Stewartson & Williams (1969), and Messiter (1970). As a first step, the linear asymptotics should be subtracted from p_{12} in order to provide a solution to be bounded at infinity. This asymptotic identically satisfies the Laplace equation and is prescribed by (5.4) along the x_i-axis. Then, the part of the pressure under examination is induced by variations of the displacement thickness which is an unknown quantity to be evaluated simultaneously with the velocity field. All other details of analysis of the potential region are omitted for brevity.

6. Locally inviscid region of the boundary layer

Let us consider most of the boundary layer extending downstream of a similar region over the smooth portion of the plate where the flow pattern is fixed by the results exposed above. Clearly, this raises the question as to what extent the velocity field changes under the effect of a surface imperfection. Advantage of (5.1*a*) is taken to scale the longitudinal coordinate, whereas the scaling $y^* = \epsilon^4 L^* y_2$ of the transverse coordinate is evident. Desired functions are presented through

$$u^* = U_\infty^* [u_{20}(y_2) + \epsilon u_{21}(t', x_i, y_2) + \ldots], \tag{6.1a}$$

$$v^* = U_\infty^* [\epsilon^2 v_{21}(t', x_i, y_2) + \ldots], \tag{6.1b}$$

$$p^* = p_\infty^* + \rho^* U_\infty^{*2} [\epsilon p_{21}(t') + \epsilon^2 p_{22}(t', x_i, y_2) + \ldots], \tag{6.1c}$$

$p_{21} = p_{11}(t')$ being known by virtue of (5.3).

As usual, a system of governing equations is cast in the form

$$\frac{\partial u_{21}}{\partial x_i} + \frac{\partial v_{21}}{\partial y_2} = 0, \quad u_{20}\frac{\partial u_{21}}{\partial x_i} + v_{21}\frac{\mathrm{d}u_{20}}{\mathrm{d}y_2} = 0, \quad \frac{\partial p_{22}}{\partial y_2} = 0,$$

however, we need to deal with the solution

$$u_{21} = A_i(t', x_i)\frac{\mathrm{d}u_{20}}{\mathrm{d}y_2} + B_i(t', y_2), \quad v_{21} = -\frac{\partial A_i}{\partial x_i}u_{20}(y_2), \tag{6.2a,b}$$

involving an additional function B_i that is zero in most cases studied so far. This function comes from matching (6.1*a–c*) as $x_i \to -\infty$ to (3.1*a–c*) where both variables x', $x_1' \to 0-$. As a result we get

$$B_i = u_{21}'(0, y_2)\, p_{11}(t'). \tag{6.3}$$

As for the instantaneous displacement $-A_i(t', x_i)$ of streamlines, it should meet the requirement $A_i \to 0$ as $x_i \to -\infty$. Since u_{21}' is in point of fact independent of x_1' on the strength of (3.4*a*) with $p_{21}' = 1$, the limit value $u_{21}'(0, y_2)$ on the right-hand side of (6.3) is merely $u_{21}'(y_2)$.

When approaching the upper edge $y_2 \to \infty$ of the boundary layer, u_{21}' experiences a singularity of order $\epsilon^{-1/2}$ whose nature was clarified in §3. The same singularity is

involved in $B_i(t', y_2)$. Hence it follows that the limit of the longitudinal velocity cannot be set by (6.2*a*) in the region where $|u_{20}(y_2)-1| = O(\epsilon^{1/2})$. On the contrary, the transverse velocity obeys (6.2*b*) everywhere within the locally inviscid deck of the boundary layer for the singularity is missing from the expression just mentioned. Matching (6.2*b*) to the relation defining the transverse velocity in the upper deck with potential flow yields

$$p_{22} = p_{12} = -\delta_0^2 \frac{4b_0 t'}{(t'^2+b_0^2)^2}\left(-\frac{1}{2b_0}+\frac{2b_0}{t'^2+b_0^2}\right)x_i - \frac{1}{\pi}\int_{-\infty}^{\infty}\frac{\partial A_i/\partial s}{s-x_i}\,\mathrm{d}s. \tag{6.4}$$

The first term on the right-hand side of (6.4) derives from the motion of the original parent vortex, the second term is typical of asymptotic problems on viscous/inviscid interaction.

7. Viscous near-wall sublayer in the vortex/roughness-interaction region

The sublayer III of figure 1, to be discussed later, is a downstream extension of the Stokes layer, the independent variables here are t', x_i, y_3. Asymptotic expansions for the desired functions read

$$u^* = U_\infty^*[\epsilon u_{30}(t', x_i, y_3)+\ldots], \tag{7.1a}$$

$$v^* = U_\infty^*[\epsilon^3 v_{30}(t', x_i, y_3)+\ldots], \tag{7.1b}$$

$$p^* = p_\infty^* + \rho^* U_\infty^{*2}[\epsilon p_{31}(t') + \epsilon^2 p_{32}(t', x_i, y_3+\ldots], \tag{7.1c}$$

with $p_{31} = p_{21} = p_{11}(t')$ being given by (5.3). Substituting (7.1*a–c*) into the initial system of Navier–Stokes equations yields

$$\frac{\partial u_{30}}{\partial x_i}+\frac{\partial v_{30}}{\partial y_3} = 0, \quad \frac{\partial p_{32}}{\partial y_3} = 0, \tag{7.2a, b}$$

$$\frac{\partial u_{30}}{\partial t'}+u_{30}\frac{\partial u_{30}}{\partial x_i}+v_{30}\frac{\partial u_{30}}{\partial y_3} = -\frac{\partial p_{32}}{\partial x_i}+\frac{\partial^2 u_{30}}{\partial y_3^2}. \tag{7.2c}$$

These are the Prandtl equations where the excess pressure p_{32} is not prescribed in advance and should be determined simultaneously with the velocity field (Stewartson 1969; Neiland 1969; Stewartson & Williams 1969; Messiter 1970).

Let us discuss the boundary conditions for the Prandtl equations. Matching (7.1*a–c*) to (4.1*a–c*) with allowance made for (4.6) leads to

$$u_{30} \to \frac{\mathrm{d}u_{20}(0)}{\mathrm{d}y_2}y_3 + p_{11}(t') + U'_{30}(t', 0, y_3) \quad \text{as} \quad x_i \to -\infty. \tag{7.3}$$

In keeping with remarks advanced in §4, we need to put $c = 1$ in the definition (5.3) of p_{11}. As for U'_{30}, this function is fixed by (4.7). On the other hand, matching (7.1*a–c*) to (6.1*a–c*) results in the limit condition at the outer edge of the viscous near-wall sublayer. With (6.2*a, b*) and (6.3) taken into consideration, the limit condition becomes

$$u_{30} - \frac{\mathrm{d}u_{20}(0)}{\mathrm{d}y_2}y_3 \to p_{11}(t') + \frac{\mathrm{d}u_{20}(0)}{\mathrm{d}y_2}A_i(t', x_i) \quad \text{as} \quad y_3 \to \infty. \tag{7.4}$$

Besides, the relations $p_{32} = p_{22} = p_{12}(t', x_i)$ arise from the matching of pressures operating across three different layers located within the viscous/inviscid interaction region at hand. These pressures involve a term with the unknown displacement

thickness, $-A_i(t', x)$, which lies at the heart of the free interaction process. The no-slip conditions

$$u_{30} = v_{30} = 0 \quad \text{at} \quad y_3 = a_i g_i(x_i), \tag{7.5}$$

make the boundary-value problem for a plate with a local hump or dent complete. The shape of the latter is given by $g_i(x_i)$, that is non-vanishing only on some interval $0 < x_i < x_{i0}$, whereas exterior to this interval $g_i = 0$. On the assumption that $\max|g_i(x_i)| = 1$, a new constant a_i serves for gauging the height or depth of the roughness.

Another approach to analysis of the free-stream vorticity propagation leading to the interaction with a boundary layer in the vicinity of a local imperfection of a flat plate has been developed by Kerschen (1989). He considered a convected gust assuming that there were no pressure fluctuations in the external velocity field. This specific vortical flow can penetrate the boundary layer on a flat plate only by viscous diffusion. The process is extremely weak at high Reynolds numbers, with the amplitude of unsteady disturbances in the near-wall sublayer being exponentially small. Here the receptivity mechanism arises solely from the distortion of the gust by an obstacle that results in the required short-scaled pressure gradients. A study by Goldstein, Leib & Cowley (1992) on a flat-plate boundary layer exposed to free-stream vorticity should be mentioned also. Their (three-dimensional) analysis shows how a small streamwise disturbance in the otherwise uniform stream ahead of a flat plate is amplified by leading-edge bluntness affects and eventually leads to a weak but nonlinear spanwise motion far downstream from the leading edge. Evidently, the aim of both works is distinct from that pursued here.

8. Boundary-value problem in canonical variables

We denote $\lambda = \mathrm{d}u_{20}(0)/\mathrm{d}y_2$ and introduce new independent variables

$$t' = \lambda^{-3/2}t, \quad x_i = \lambda^{-5/4}x, \quad y_3 = \lambda^{-3/4}[y + ag(x)], \tag{8.1a–c}$$

with $a_i = \lambda^{-3/4}a$ and $g_i = g(x)$ that is non-vanishing only over the segment $0 < x < x_0, x_{i0} = \lambda^{-5/4}x_0$. As for the desired functions, they are defined by means of

$$u_{30} = \lambda^{1/4}u(t, x, y), \quad v_{30} = \lambda^{3/4}\left[v(t, x, y) + a\frac{\mathrm{d}g}{\mathrm{d}x}u(t, x, y)\right], \tag{8.2a, b}$$

$$p_{32} = \lambda^{-1/2}\left[-\frac{dp_v}{\mathrm{d}t}x + p_i(t, x)\right], \tag{8.2c}$$

$$p_v = p_v(t) = -\tfrac{1}{2}\delta^2\left[\left(-\frac{1}{2b} + \frac{2b}{t^2 + b^2}\right)^2 - \left(\frac{1}{2b}\right)^2\right]. \tag{8.2d}$$

The constants b and δ entering the right-hand side of (8.2d) for the vortex-induced pressure p_v are given by

$$b_0 = \lambda^{-3/4}b, \quad \delta_0 = \lambda^{-11/8}\delta. \tag{8.3a, b}$$

Substituting (8.1a–c) and (8.2a–d) into (7.2a–c) yields

$$\frac{\partial u}{\partial x} + \frac{\partial v}{\partial y} = 0, \quad \frac{\partial p_i}{\partial y} = 0, \tag{8.4a, b}$$

$$\frac{\partial u}{\partial t} + u\frac{\partial u}{\partial x} + v\frac{\partial u}{\partial y} = \frac{\mathrm{d}p_v}{\mathrm{d}t} - \frac{\partial p_i}{\partial x} + \frac{\partial^2 u}{\partial y^2}. \tag{8.4c}$$

Here the pressure gradient consists of two terms. The first one, $\mathrm{d}p_v/\mathrm{d}t$, depending on time only derives from the motion of the original parent vortex, the second term, $\partial p_i/\partial x$, is the contribution to the pressure gradient from the vortex/roughness interaction resulting in sharp variations of the instantaneous displacement thickness, $-A(t,x)$. In accordance with (6.4) and (8.2*c*) the self-induced pressure takes on the form

$$p_i = \frac{1}{\pi}\int_{-\infty}^{\infty} \frac{a\,\mathrm{d}g/\mathrm{d}s - \partial A/\partial s}{x-s}\,\mathrm{d}s. \tag{8.5}$$

Now we turn to the boundary conditions which also involve the displacement thickness sought for. The asymptotic behaviour of the near-wall sublayer in the limit as $x_i \to -\infty$ essentially depends on $U'_{30}(t',0,y_3)$ in view of (7.3). This function is a solution to the classical heat-conduction equation. The latter remains invariant under the affine transformation (8.1*a*, *c*) of t', y_3 hence (7.3) reduces to

$$u \to y + p_v(t) + U_{30}(t,y) \quad \text{as} \quad x \to -\infty. \tag{8.6}$$

The form of U_{30} on the right-hand side of (8.6) is obtainable from (4.7) as

$$U_{30} = -\frac{1}{2\pi^{1/2}}\int_{-\infty}^{t} \frac{y}{(t-\tau)^{3/2}}\exp\left[-\frac{y^2}{4(t-\tau)}\right]p_v(\tau)\,\mathrm{d}\tau, \tag{8.7}$$

with allowance made for the fact that $g(-\infty) = 0$. In canonical variables the limit condition (7.4) at the upper reaches of the viscous near-wall sublayer reads

$$u - y \to p_v(t) + A(t,x) \quad \text{as} \quad y \to \infty. \tag{8.8}$$

Finally, the no-slip conditions (7.5) are written in the standard form

$$u = v = 0 \quad \text{at} \quad y = 0, \tag{8.9}$$

owing to a shift (8.1*c*) in the transverse coordinate.

Thus, the fluid motion obeys the Prandtl equations (8.4*a*–*c*) with the pressure gradient consisting of a prescribed quantity $\mathrm{d}p_v/\mathrm{d}t$ and a part $\partial p_i/\partial x$ sought for. By virtue of (8.5), the latter depends, in turn, both on the roughness shape fixed by $g(x)$ and the instantaneous displacement thickness, $-A(t,x)$. The total number of the similarity parameters determining the flow pattern is four. Two of them, the strength δ of the vortex filament and the distance b separating it from the wall, serve to specify p_v as a function of time which enters the boundary conditions (8.6) and (8.8) as well. Two additional parameters, the height (or depth) a of the obstacle and its length x_0, are found only in (8.5), they are missing from the boundary conditions. It is worthy of note that U_{30} evaluated from the velocity field within the Stokes layer depends on the first pair of parameters, δ and b, for the kernel of an integral on the right-hand side of (8.7) is expressed through p_v. The only similarity parameter appears in a simpler version of the problem on the boundary layer induced by a convected vortex over an infinite flat plate (Doligalski & Walker 1984).

9. Analogy with sound scattering

The interaction of an acoustic wave travelling along a plate with an obstacle placed at some station from the leading edge is to a large extent similar to that set forth above. Harmonic oscillations have been studied by Ruban (1984), Goldstein (1985), and

Goldstein & Hultgren (1987, 1989), however the closest resemblance shows the propagation of a sound pulse. Features peculiar to this phenomenon stem from three sources. First, a fluid in the potential flow region cannot be considered to be incompressible even if velocities are small everywhere. This implies the necessity of incorporating the Mach number M_∞ into a set of similarity parameters. Secondly, unlike a vortex stuck with some particular fluid particle, an acoustic pulse propagates relative to the same particles with the speed of sound. Thirdly, it follows that a relationship between the excess pressure and particle velocities in an acoustic wave is linear (more precisely, this relationship is the same as that inherent in the Riemann travelling wave). The latter point is crucial, for it allows us to simplify significantly the analysis of the flow in a region upstream of a local roughness. Omitting details let us present an extension of results by Ruban (1984), Goldstein (1985), and Goldstein & Hultgren (1989) as applied to signals of the pulse mode.

We begin with a remark that the short-scaled variable is defined as $X = M_\infty x' - (1 + M_\infty) t'$ where the non-dimensional time t' and longitudinal coordinate x' are introduced by (2.2a, b). Similar to (2.6a), the excess pressure proves to be proportional to ϵ, however, $p_1'(t', x')$ is an arbitrary function of X expressed in terms of the perturbed velocity simply through $p_1' = M_\infty^{-1} u_1'(t', x')$. Then, an expression $P = P(X) = p_1'(t', x')$ holds true for a function entering the right-hand side of (3.1c). Owing to a linear dependence relating the excess pressure to the perturbed velocity in the external region of the fluid motion, a solution to the system of equations for u_{21}' and v_{21}' remains regular when approaching the upper reaches of the boundary layer as opposed to (3.4a, b) with a singularity becoming operative as $y_2 \to \infty$. As a result, we do not need to perform a separate analysis that leans upon going over into a moving frame of reference in order to take advantage of the Bernoulli integral. The governing equation (4.3) still stands for sound-pulse scattering, a solution sought for takes on the form (4.6). This suggests that the last term U_{30}' there satisfies the classical heat-conduction equation in t' and y_3 and is obtainable from (4.7) within an accuracy of some constant multipliers. Thus, the structure of a region upstream of the surface imperfection is worked out.

Let us set about posing a boundary-value problem for the viscous near-wall sublayer interacting with an acoustic pulse in the region where a local roughness springs up. When the independent variables and desired functions are affine transformed in a manner analogous to (8.1a–c), (8.2a–d), the system of governing equations becomes (8.4a–c) with $p_v = P(-\omega t)$. As before, this part of the excess pressure involves two similarity parameters, δ and ω. Noteworthy is, however, the fact that the reduced amplitude of incident sound disturbances is proportional to δ rather than δ^2, as it was the case in the vortex/obstacle interaction process. The frequency parameter ω essentially depends on M_∞ and arises in place of a distance b separating the vortex from a plate by (8.3a). As for another part p_i of the excess pressure, the previous definition (8.5) still stands for it and contains two more similarity parameters, a and x_0.

In conclusion, we discuss briefly boundary conditions. At the entry $x \to -\infty$ into the viscous near-wall sublayer, the limit relation (8.6) with a function

$$U_{30} = U_{30}(\omega t, \omega^{1/2} y) \tag{9.1}$$

holds and at the upper reaches of this sublayer, (8.8) may be applied. As an example let the pressure in a sound pulse be given by means of the δ-function, then

$$U_{30} = -\frac{1}{2\pi^{1/2}} \frac{\delta}{\omega} \frac{y}{t^{3/2}} \exp\left(-\frac{y^2}{4t}\right) \quad \text{for} \quad t > 0,$$

on the strength of (8.7) and (9.1). So, in the simplest case under consideration, U_{30} is a heat dipole with the moment

$$I(t) = \int_0^\infty y U_{30}(t, y)\,\mathrm{d}y,$$

preserved constant in time. The no-slip conditions on the plate with a bump or dent are fixed by (8.9).

Scattering of harmonic acoustic waves impinging at an angle on the boundary layer over a plate has been studied by Kerschen (1989) and Heinrich & Kerschen (1989). This process is more complicated than that examined above since disturbances in the vicinity of the leading edge need to be analysed separately. Results related to the latter effect are summarized in Goldstein & Hultgren (1989).

10. Computations of vortex/roughness interaction

Numerical solutions of the nonlinear boundary-value problem posed in §8 are intended to trace the evolution of the disturbance pattern depending on the potential vortex intensity. The basis for computed results described below is the pseudospectral scheme which was first developed in Burggraf & Duck (1982) and Duck (1987). It was employed to evaluate unsteady disturbed flows within the framework of both the triple-deck theory (Duck 1985, 1988; Ryzhov & Savenkov 1989, 1991) and interacting boundary-layer approach (Chuang & Conlisk 1989). Owing to the FFT algorithm incorporated, this technique treats reversed-flow bubbles correctly without the need for any kind of approximation or adaptation typical of conventional finite-difference schemes. Our experience suggests also that the pseudospectral method is less time-consuming, for approximately half the number of grid points are necessary to bring the results to within a few per cent of the corresponding values calculated by means of finite-difference schemes. Similar conclusions have been drawn by Chuang & Conlisk (1989). A comprehensive comparison of the two numerical procedures is available in the recent study of Bodonyi *et al.* (1989). Thus, with spectral computation, tolerable accuracy in final prediction can be achieved using moderate machines. Insofar as all the details of the numerical method in question are well documented now they will be omitted here. However, it is worthy of note that spectral computation provides not only physical quantities but their Fourier decompositions in the wavenumber space also. As we shall see, this additional information is extremely helpful for understanding the essence of the nonlinear process under consideration.

In line with Burggraf & Duck (1982) and Duck (1985, 1987) the system of Prandtl equations is transformed by introducing a shear stress $\tau = \partial u/\partial y$ as a new desired function, the same substitution is applied to recast the boundary conditions. The shear stress plays a dominant part in constructing an iteration procedure. Thus, the boundary-value problem reduces in point of fact to computing the Fourier spectrum

$$\bar{\tau}(t, k, y) = \int_{-\infty}^{\infty} \tau(t, x, y)\,\mathrm{e}^{-\mathrm{i}kx}\,\mathrm{d}x, \tag{10.1}$$

and then inverting it to yield a distribution

$$\tau(t, x, y) = \frac{\partial u(t, x, y)}{\partial y} = \frac{1}{2\pi}\int_{-\infty}^{\infty} \bar{\tau}(t, k, y)\,\mathrm{e}^{\mathrm{i}kx}\,\mathrm{d}k, \tag{10.2}$$

of the shear stress in the physical space. Our prime interest is in the variation of $\tau_w = \tau(t, x, 0)$ as a function of x with t taking on successively increasing values. Mention may be made in this connection that separation of a steady boundary layer is fixed by a passage of τ_w through zero.

A code with the FFT algorithm underlying the nonlinear calculations was tested in Ryzhov & Savenkov (1989) when analysing the soliton nature inherent in central cycles of oscillations in a wave packet entering a large-amplitude stage of evolution. It proved to be highly efficient even though the calculations were carried out using moderate machines. However, the code was modified in such a way that a tridiagonal matrix became characteristic of the iteration process to make the overall numerical technique as simple as possible. A transformation (Burggraf & Duck 1982; Duck 1985)

$$y = h(\eta), \quad h = \frac{\eta}{1-\eta}, \tag{10.3}$$

of the normal coordinate remains to be mentioned in connection with previous work, for the experience available suggests that a compressed/stretched grid in the transverse direction may essentially increase accuracy when solving an equation for $\bar{\tau}$. The sizes of the computational domain and steps in space were chosen as follows. For a timestep $\Delta t = 0.005$, the number N_k of mesh points in the spectral space was $N_k = 256 = 2^8$ to meet the constraints of the FFT algorithm. A limitation $\max k = 25.6$ turned out to be not too rigid and resulted in a step $\Delta k = 0.1$ in the wavenumber k. On the strength of (10.1), (10.2), we may estimate the length l_x of an interval in the longitudinal coordinate as $l_x = 62.8$ with the corresponding step $\Delta x = 0.1227$. The equation for $\bar{\tau}$ was solved over the range $0 \leqslant \eta \leqslant \eta_\infty = 0.95$, as a consequence an upper bound $y_\infty = 19$ for y emerged. A step $\Delta\eta = 0.04$ was fixed by 25 mesh points at each $(k, t-\frac{1}{2}\Delta t)$-station. It is worth noting that this choice of the finite-difference scheme parameters fixes lesser values of steps in time as well as in physical and spectral spaces than those used in most of the computations in the aforementioned papers. Therefore, in all examples presented below, only 5–6 iterations were necessary to provide convergence in computing nonlinear terms on the right-hand side of the equation for $\bar{\tau}$. Once convergence (defined by the maximum change of 10^{-5} in the pressure) was achieved, the calculation was carried on to the next timestep. For the purpose of checking the accuracy, some other grids were used giving graphically indistinguishable results (not presented here).

In numerical analysis of the convected vortex/boundary-layer interaction a hump of the form

$$g = \frac{1}{1+x^2}, \quad \bar{g} = \pi \mathrm{e}^{-|k|}, \tag{10.4}$$

was assumed to be mounted on an otherwise flat plate, the height of the obstacle being $a = 1$. The distribution of the disturbed wall shear stress $\tau_w^d = \tau_w - 1$ in a steady flow set in prior to the vortex motion is plotted in figure 2(*a*), whereas its Fourier transform $|\bar{\tau}_w^d|$ can be seen in figure 2(*b*). We emphasize at this point that for better visualization of oscillation properties a quantity $\tau_w^d = \tau_w - 1 - \partial U_{30}/\partial y$ is generally meant by τ_w^d in what follows. This quantity coincides with $\tau_w^d = \tau_w - 1$ for the steady flow in the absence of the vortex inducing an additional component, U_{30}, of velocity. The hump under discussion brings about moderate (though finite) variations in the velocity field of the oncoming stream that do not provoke separation accompanied by a bubble with reversed flow. Supposedly, the resulting boundary-value problem is relevant to gas-turbine-engine environment where vortical disturbances interact with small imper-

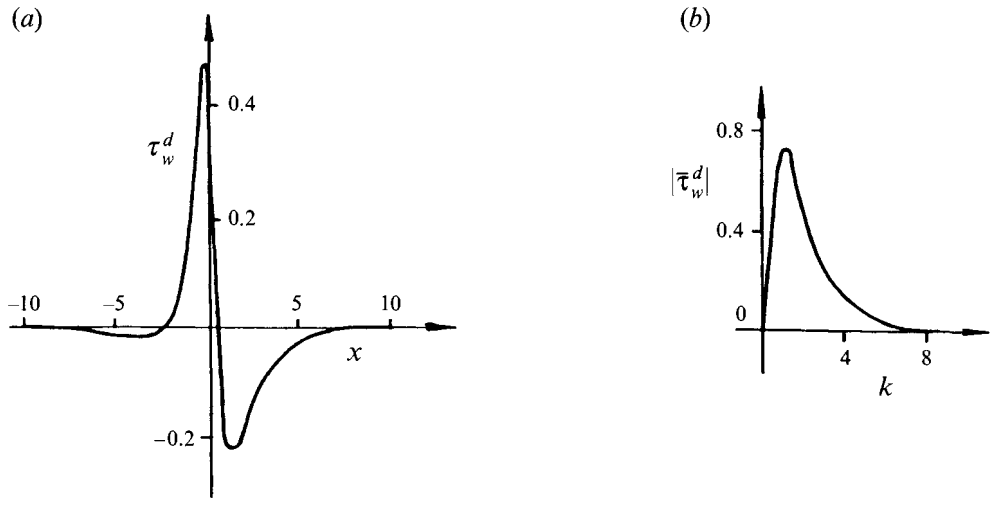

FIGURE 2. Wall shear stress and its spectrum for the steady flow over a hump whose shape is given by (10.4) with $a = 1$. (*a*) Distribution of $\tau_w^d = \tau_w - 1$ against x. (*b*) Absolute value $|\bar{\tau}_w^d|$ of the Fourier transform $\bar{\tau}_w^d$ versus the wavenumber k.

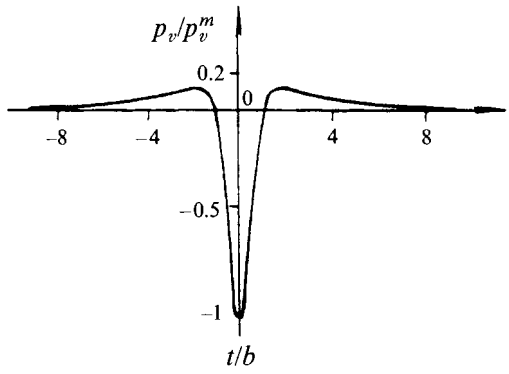

FIGURE 3. Variation of the vortex-induced pressure with time at the central point of the hump; p_v^m is the maximum of $|p_v|$, b designates a distance separating the vortex from the plate.

fections of the turbine-blade surface (see, for example, Mayle 1991). The interaction process triggered by a potential vortex travelling over a larger-sized hump with a separation region downstream of it calls for an additional study and work is in progress now.

For better visualization of how the vortex-induced pressure p_v varies in time, let us rewrite (8.2*d*) as

$$p_v = -\tfrac{1}{2}p_v^m\left\{\left[-\tfrac{1}{2}+\frac{2}{1+(t/b)^2}\right]^2-\tfrac{1}{4}\right\}, \quad p_v^m = \max|p_v| = \left(\frac{\delta}{b}\right)^2. \tag{10.5}$$

The plot of p_v/p_v^m as a function of t/b is shown in figure 3. If the vortex strength is taken to be $\delta = 0.1$, then $p_v^m = 1$ for the distance $b = 0.1$ separating the vortex from the plate. With δ fixed, variations of the vortex-induced pressure are provoked by the separating distance b. Let the convective vortex be elevated at a large height above the wall,

resulting in the first limit case $b \gg 1$. As we can see from (10.5), the positive wings in the induced-pressure distribution are of considerable importance since they interact with a roughness on a timescale estimated as $t = 0(b) \gg 1$. Although the pressure variations in the wings are relatively small, they give rise to disturbances exponentially growing with time according to linear stability theory (Ryzhov & Terent'ev 1984; Ryzhov 1989; Kozlov & Ryzhov 1990). Therefore, by the instant $t = 0$ the amplitude of these disturbances can exceed the amplitude of pulsations which start to develop under the influence of the negative peak in the pressure distribution. By contrast, with the vortex travelling at a small height above the wall, we are led to the second limit case $b \ll 1$. The role played by the long wings in the pressure distribution is herein decreased because the timescale of their interaction with an obstacle falls up to order $t = 0(b) \ll 1$ in magnitude. By the instant $t = 0$ disturbances generated earlier have not managed to evolve to an extent that they may distort the structure of a wave packet triggered by the central peak of the pressure. The same conclusions are derivable using a study of the vortex-induced velocity fields in Doligalski & Walker (1984).

Allowance for the mechanism underlying the vortex/roughness interaction was included in the numerical algorithm. Time in the iteration process was counted from $t_0 = -3$. Special tests confirmed that computed results were not affected by this particular choice of the initial instant. What is more, frictional intensities calculated at $t = -1$ appeared to be practically identical to those prescribed at $t_0 = -3$. The wings in the vortex-induced pressure exert some influence on the shape of oscillations, emitted in the course of interaction, which is hardly accounted for. In order to eliminate this influence from the following analysis of disturbance propagation or reduce it to a minimum, the distance separating the vortex from the plate was taken fairly small (as mentioned above, $b = 0.1$).

First of all, it is advisable to make a comparison between results of linear and nonlinear studies of the interaction process under examination. Let us put $\delta = (0.1)^{1/2} \times 10^{-1}$, whence $p_v^m = 10^{-1}$. With this value of the vortex strength, the system of equations (8.4*a–c*) can be linearized around the basic steady flow marked by distributions τ_w^d, $|\bar{\tau}_w^d|$ in figures 2(*a*) and 2(*b*), respectively. The shape of disturbances emitted is shown in figure 4(*a*) for $t = 3$ whereas figure 4(*b*) illustrates their spectral content; in both cases a solid line relates to the nonlinear solution, a dotted line is drawn according to the data from a linear approach. This is a typical wave packet that was generated during convected vortex/hump interaction and then broke away from the obstacle when moving downstream. An oscillation pattern of this type is in full agreement with the general concept of boundary-layer receptivity to disturbances of a different physical nature (Goldstein & Hultgren 1989; Kerschen 1989; Ryzhov 1989; Kozlov & Ryzhov 1990). It is worthy of notice that accounting for nonlinear effects at an earlier stage under discussion makes the amplitude of several central cycles of pulsations grow faster whilst the amplitude of oscillations advanced to form a long 'wave tongue' of the modulated signal turns out to be practically identical in the framework of both linear and nonlinear approaches. The spectrum $|\bar{\tau}_w^d|$ merits notice also: the first smoothed-out maximum here is apparently associated with a steady flow past the same obstacle (cf. figure 2*b*), the second forked maximum made up of two peaks features the phenomenon at hand in nonlinear formulation. The position of these two peaks around the wavenumber $k = 2.75$ corresponding to the fastest growing mode of linear disturbances is typically occupied by another smoothed-out maximum which is responsible for amplitude-modulated oscillations within a weak wave packet (Ryzhov & Terent'ev 1986; Ryzhov & Savenkov 1989, 1991; Kozlov & Ryzhov 1990). The splitting of the second maximum and wiggles in the decaying part of $|\bar{\tau}_w^d|$ arise from

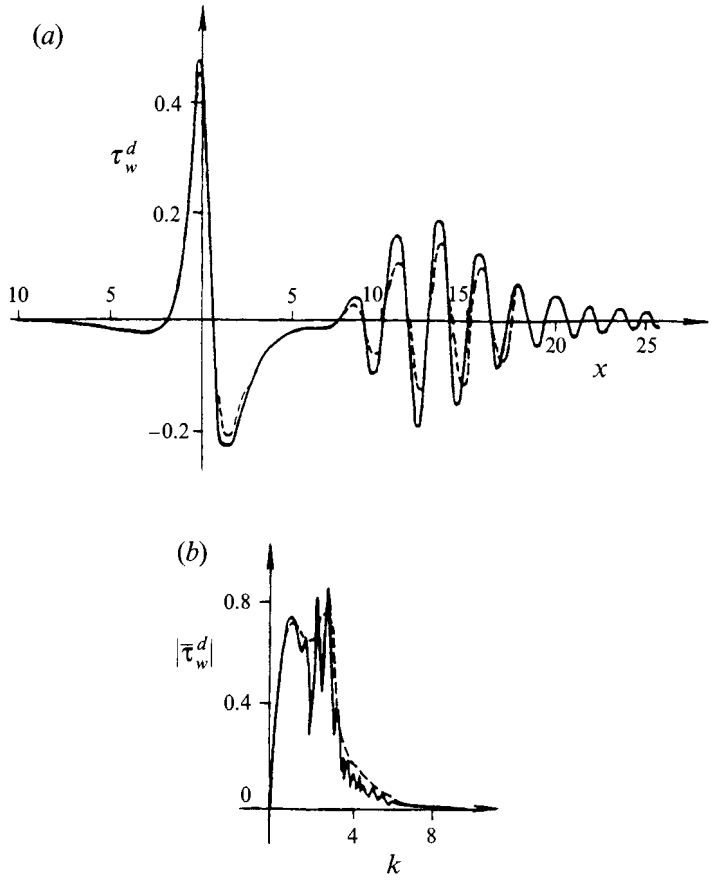

FIGURE 4. Wall shear stress and its spectrum for a wave packet generated by a weaker vortex of $p_v^m = 10^{-1}$ at $t = 3$; ---, linear approach; ——, nonlinear calculations., (*a*) Distribution of $\tau_w^d = \tau_w - 1 - \partial U_{30}/\partial y$, where U_{30} is the vortex-induced velocity defined in (8.7), against x. (*b*) Fourier transform $|\bar{\tau}_w^d|$ versus the wavenumber k; the first smoothed-out maximum is associated with the steady flow, the subsequent maximum near $k = 2.75$ appearing as fork-shaped in nonlinear calculations corresponds to the fastest growing mode of linear disturbances.

sums and differences of the wavenumbers characteristic of the steady velocity field and most unstable Tollmien–Schlichting modes. However, these nonlinear effects do not lead to short-scaled distortions in the signal shape.

Let us enhance the vortex-filament strength choosing $\delta = 10^{-1}$ with a consequence that $p_v^m = 1$ and an initial value $p_v(-3) = -5.5 \times 10^{-4}$. As seen from figure 5(*a*), at the time $t = 1$ the wave packet is of a fairly developed shape but still inextricably entwined with steady disturbances of the boundary layer centred around the hump. A plot of the spectrum in figure 5(*b*) corresponds to this stage of disturbance evolution. The two maxima following each other exert control over the wall-shear-stress distributions in the steady flow and wave packet, respectively. It is obvious that an increase of $|\bar{\tau}_w^d|$ when the wavenumber approaches a value $k = 5.5$ is brought about by the start of the nonlinear process. Owing to nonlinearity, along with vigorously growing modes from the vicinity of $k = 2.75$, modes with the wavenumbers doubled become amplified as well. However, the spectrum $|\bar{\tau}_w^d|$ has two more local maxima over the range $2.75 < k < 5.5$. They arise from a fairly complicated interaction of steady disturbances with pulsations induced by the convected vortex. The very generation of both maxima

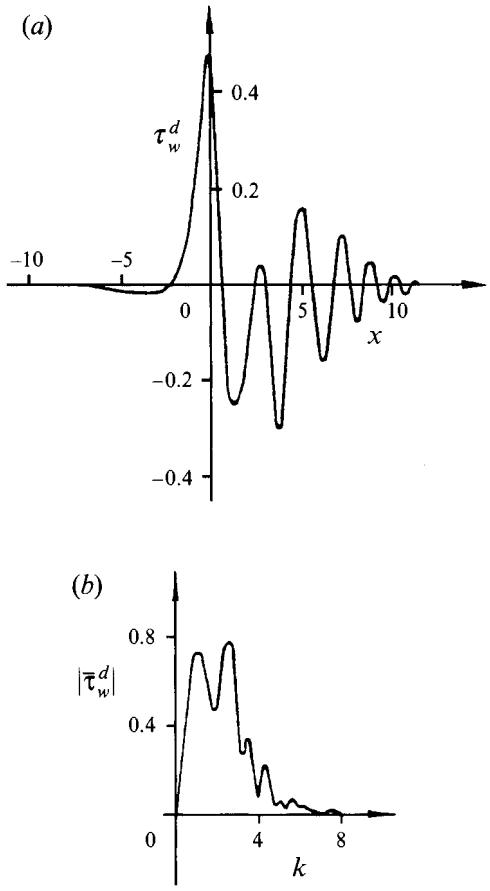

FIGURE 5. Wall shear stress and its spectrum for a wave packet generated by a vortex of the moderate strength $p_v^m = 1$ at $t = 1$. (*a*) Distribution of τ_w^d against x shows a fairly developed oscillation pattern to be inextricably entwined with steady disturbances. (*b*) Fourier transform $|\bar{\tau}_w^d|$ versus the wavenumber k with two maxima controlling the disturbed steady flow and the wave-packet emission.

and small-amplitude wiggles with $k > 5.5$ can be inferred in the same way as has been used in the above discussion of the spectrum in figure 4(*b*). However, irregularities in the spectral space are found to be more flattened now.

Figures 6(*a*) and 6(*b*) show the same wave packet with $p_v^m = 1$ and its spectrum at $t = 3$, i.e. at an instant which was chosen above for discussing weaker (nearly linear) disturbances illustrated by figures 4(*a*) and 4(*b*). A nonlinear character of oscillations clearly manifests itself in cycles with the largest amplitude (of order 3). The parts of two central cycles with negative wall shear stress are narrower as compared to these parts where the frictional intensity is positive. The pulsation swing in the negative phases of each cycle is greater than that attained in the positive phases. This is a typical feature of the soliton nature of nonlinear disturbances propagating through a boundary layer. In connection with the wave-packet structure, soliton properties were first recognized by Ryzhov & Savenkov (1989); their importance for explanation of the *K*-type of laminar boundary-layer breakdown was indicated in Ryzhov (1990) and discussed in detail by Kachanov, Ryzhov and Smith (1993) using both theoretical concepts (in the framework of the Benjamin–Ono equation) and experimental evidence. The formation of spikes in regions with positive values of τ_w is also intrinsic to the phenomenon in question. The emergence of these spikes marks the onset of a

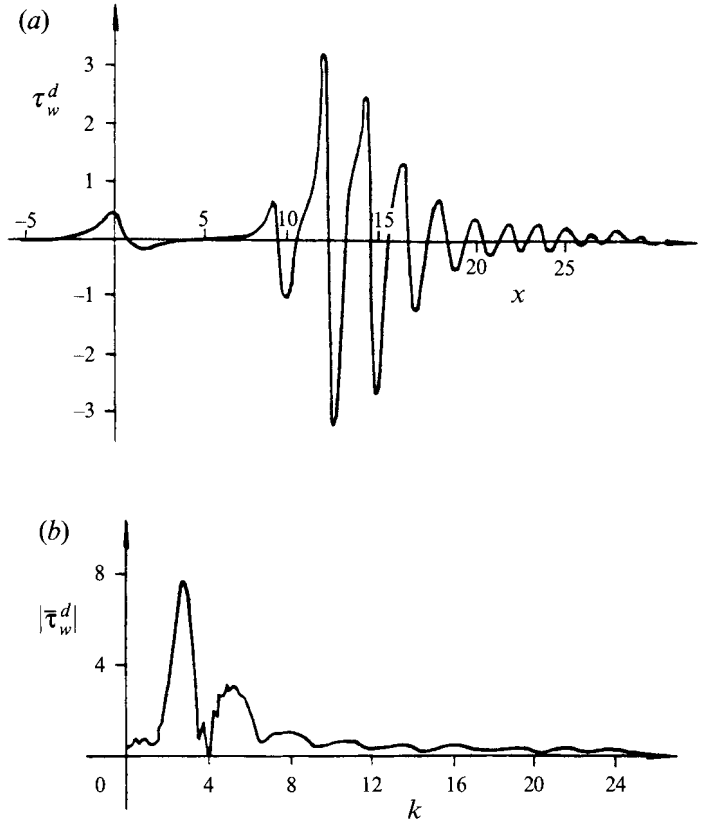

FIGURE 6. The same wave packet and its spectral content at a later instant $t = 3$. (*a*) Distribution of τ_w^d against x exhibits spiky oscillations of much larger amplitude as compared with steady disturbances. (*b*) Fourier transform $|\bar{\tau}_w^d|$ versus the wavenumber k contains local maxima derived from the modes of multiplicity 2 to 5 of the most amplifying linear wave.

transitional process terminating in the blow-up of the regular pattern of the wave packet. On the other hand, disturbances of the smaller amplitude which are travelling at higher speed in front of the wave packet obey the linear laws. Nevertheless, the regime as a whole may be regarded as one where the boundary-layer receptivity to an external convected vortex is responsible for emission of a moderately nonlinear wave packet close to the plate imperfection.

The following comments are in order with regard to the spectral curve in figure 6(*b*). First, the height of the major maximum around $k = 2.75$ increased approximately by a factor of 10 in the time interval $\Delta t = 2$ under consideration, whilst the distribution of $|\bar{\tau}_w^d|$ in a long-wave (small k) part of the spectrum did not substantially change. This was not surprising because the part of the spectrum mentioned is primarily responsible for the steady velocity field close to an obstacle. With the major maximum drastically enhanced, wiggles in the spectral intensity proved to be much weaker as compared with irregularities featuring the behaviour of $|\bar{\tau}_w^d|$ in figure 4(*b*) for $p_v^m = 10^{-1}$ at the same instant $t = 3$. Then, amplification of modes with doubled values of the wavenumbers in the vicinity of $k = 5.5$ became more acutely pronounced, but in addition to them modes of higher multiplicity came into operation and began to grow. Clearly discernible local maxima in $|\bar{\tau}_w^d|$ derive from the modes of multiplicity 3, 4 and 5. The new maxima are gently sloping and intervals with $|\bar{\tau}_w^d| = 0$ are missing in between, i.e.

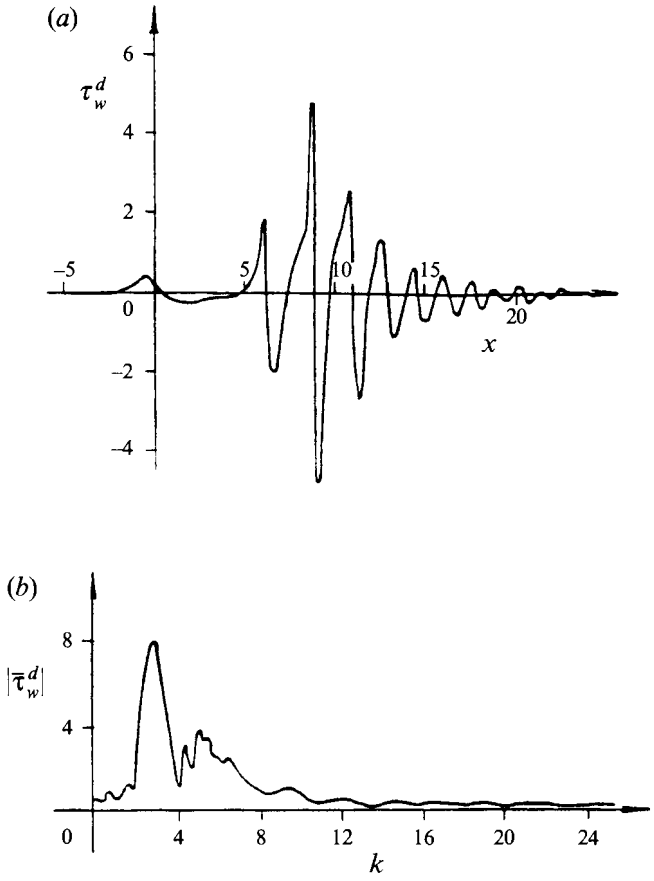

FIGURE 7. Wall shear stress and its spectrum for a wave packet generated by a stronger vortex of $p_v^m = 3$ at $t = 2$. (*a*) Distribution of τ_w^d against x gives a picture of large-sized nonlinear pulsations which become fully detached in the close vicinity of the hump. (*b*) Fourier transform $|\bar{\tau}_w^d|$ versus the wavenumber k with several small local maxima in the range $4 < k < 8$ ensuing from the complicated interaction of the convected vortex with the steady inhomogeneous velocity field.

the filling of the spectrum takes place in an almost continuous manner. Owing to this feature the earlier stage of the wave-packet breakdown quickly terminates in a blow-up of the modulated signal. However, mention should be made that subharmonic modes of multiplicity $\frac{1}{2}$ are not excited in two-dimensional disturbances. The subharmonic resonance is apparently intrinsic in three-dimensional oscillations only. The first experimental evidence providing strong support for this view was obtained by Gaster & Grant (1975). The development of localized disturbances in a boundary layer from a small-amplitude wave-packet stage up to the ultimate formation of a turbulent spot was traced in low-turbulence wind-tunnel tests by Cohen *et al.* (1991).

The explosive character of the modulated signal propagation is further illustrated by the computation of a vortex filament of still greater intensity for which purpose we put $\delta = \sqrt{3} \times 10^{-1}$ and, respectively, $p_v^m = 3$, $p_v(-3) = -1.65 \times 10^{-3}$. The wave packet shown in figure 7(*a*) at the time $t = 2$ bears the same distinctive features as that discussed above, but the pulsation swing within its central cycles increases appreciably (the maximum amplitude becomes of order 5). The spectral curve in figure 7(*b*) involves an acutely pronounced maximum close to $k = 2.75$, corresponding to the most amplified modes of linear oscillations, and a slightly bifurcated maximum with doubled

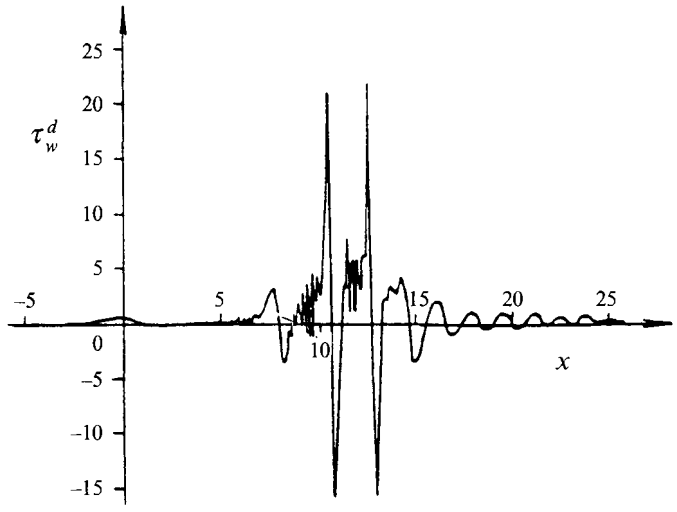

FIGURE 8. The same wave packet at a later instant $t = 2.5$ with undistorted soliton-like negative phases and sharp spikes accompanied by short-scaled wiggles arising in the positive phases of two central cycles.

values of the wavenumbers in the vicinity of $k = 5.5$. Yet another maximum is located in between, it derives from complicated interaction of the vortex filament with an inhomogeneous velocity field around the hump on the flat plate. Thus, the spectral curve $|\bar{\tau}_w^d|$ in figure 7(*b*) behaves very much like analogous distributions inherent in the linear stage of disturbance evolution (figure 4*b*) as well as in the onset of the nonlinear process (figure 5*b*). Our concern is, however, with a distant part of the spectrum specified by $k > 5.5$. Though gently sloping and flattened maxima with three-, four-, and five-fold values of the wavenumbers are clearly discernible in the general run of the curve, these parts of the spectrum merge together leaving no empty intervals with $|\bar{\tau}_w^d| = 0$. Furthermore, oscillations are excited over the range $15 < k \leqslant 25$ (actually limited by a code in operation). The spectrum becomes truly continuous pointing to the fact that the wave packet enters a final stage where its regular pattern breaks down. The excitation of distant parts of the spectrum with $k \gg 1$ for disturbances of large amplitude emitted under different circumstances has been registered also in computations by Duck (1987, 1988) and Bodonyi *et al.* (1989).

Further computation soon becomes unreliable using parameters of the code indicated above. First, a wavenumber range $0 \leqslant k \leqslant 25$ should be extended whereas a step-size $\Delta k = 0.1$ in the spectral space needs to be made smaller. However, qualitative trends to dominate the ensuing evolution of the wave process may well be brought to light with finite-difference scheme parameters kept unchanged up to the instant $t = 2.5$. Figure 8 illustrates the overall structure of localized disturbances. Characteristic of the terminal stage is an intensive and yet smooth growth of the negative 'soliton' phases of two central cycles, in spite of their large (of order 15) amplitude. As for the positive phases of the same cycles, they are completely distorted exhibiting extremely sharp spikes and wiggles which come about under the influence of a short-wave part of the spectrum with $10 < k \leqslant 25$. One more spike takes shape in the positive phase of another cycle moving somewhat faster in front of these two. The tendency toward instability of positive phases in the wall-shear-stress distributions vigorously affected by spike formation has been revealed by Ryzhov & Savenkov (1989) when processing numerical data related to a slightly earlier stage of a wave-packet propagation under

different circumstances (see also Smith 1991). As we see, the same tendency features the process of convected vortex/small roughness interaction. According to Chuang & Conlisk (1989), wiggles appear as well when the vortex strength gets sufficiently high to provoke the singular focusing of a tertiary eddy generated in the interacting boundary layer. In the present example, the characteristic length peculiar to the negative 'soliton' phases of central cycles remains in effect unchanged with time varying through a range $2 \leqslant t \leqslant 2.5$, however, the positive phases are being filled by short-scaled large-amplitude pulsations. A possible explanation for this effect is the onset of a Rayleigh instability triggered on a streamwise lengthscale much shorter than that underlying the triple-deck theory (Smith & Bodonyi 1985), though inviscid instabilities may persist within the full triple-deck formulation under discussion here (Tutty & Cowley 1986). A careful analysis by Duck (1988) lends credence to the view that Rayleigh modes may enter calculations and affect disturbance breakdown. In turn, an abrupt decrease in the streamwise lengthscale of oscillations calls for revising key assumptions of an asymptotic theory based on the boundary-layer concepts, and allowance for the normal pressure gradient should be made first of all (Ryzhov 1993).

11. Sound scattering computations

As was mentioned in §9, there is the exact analogy between the convected vortex/surface-roughness interaction and sound scattering into Tollmien–Schlichting waves by inhomogeneities embedded in a steady velocity field (for a review of the latter topic see, for example, Goldstein & Hultgren 1989). What is more, the form $f(t) = P(-\omega t)$ of a sound pulse can be chosen in such a way as to render it identical to a function $p_v(t)$ defined by (8.2d). This enables the vortex motion and interaction to be modelled by means of acoustic generators. The reverse does not hold, however, because sound disturbance may be given an arbitrary shape.

Let us describe in brief computational results on modulated oscillations in the boundary layer provided that

$$f = \delta t \exp(-\omega t), \quad (t \geqslant 0), \tag{11.1}$$

and $f = 0$ for all $t < 0$. Here the values of parameters are fixed by $\delta = 0.1e/\omega$ and $\omega = 5.765$, the obstacle being specified through (10.4) and $a = 1$. As distinct from a sharp peak with gently sloping wings on each side of it which are characteristic of the pressure distribution in figure 3, a function $p_v = f(t)$ in the case in question is positively defined for any $t > 0$, a plot of this function is presented in figure 9. With the values of parameters indicated we get $p_v^m = 0.1$. As a result sound scattering gives rise to weak vortical disturbances. The wave packet emitted during interaction enters an essentially nonlinear stage at approximately $t = 5$ and figures 10(a) and 10(b) show the distributions of τ_w^d and $|\bar{\tau}_w^d|$, respectively, for this particular instant. In spite of the fact that the modulated signal is generated by a pulse with the positive excess pressure, the oscillation pattern does not change. In all essential features the wave packet bears a close resemblance to those depicted in figures 6(a) and 7(a). As for the spectral function $|\bar{\tau}_w^d|$, its main maximum is somewhat shifted from $k = 2.75$ towards lesser values of the wavenumbers, and other local maxima for modes of multiplicity 2 to 6 stand out clearly. A shift in the position of the main maximum derives from actual nonlinearity of the process leading to localized disturbance generation. Though the process as a whole depends on the precise form of p_v, this dependence, as the computation suggests, is weak for the hump (10.4) with $a = 1$ in the present example.

The last example relates to the wave-packet emission during sound scattering on a

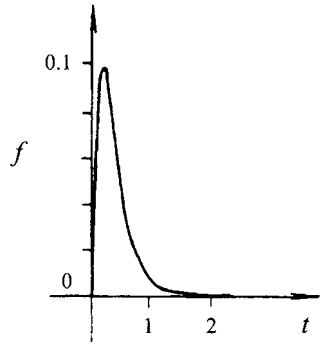

FIGURE 9. Variation of the excess pressure with time in an incident positive sound pulse fixed by (11.1) with $p_v^m = 10^{-1}$.

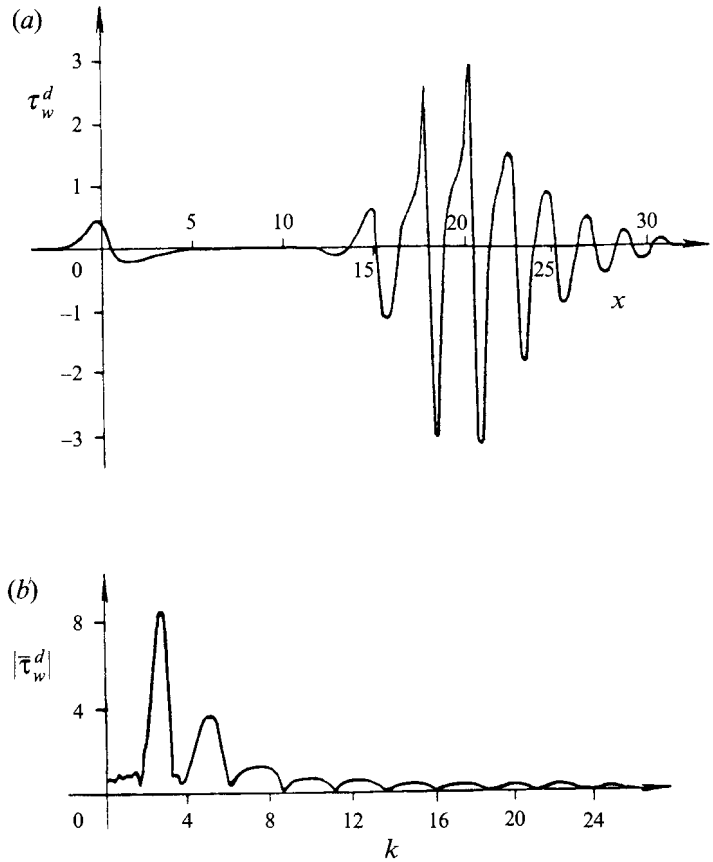

FIGURE 10. Wall shear stress and its spectrum for a wave packet generated by the sound pulse (11.1) when impinging on the hump, given in (10.4) with $a = 1$, at $t = 5$. (*a*) Distribution of τ_w^d against x is very similar to that plotted in figure 5(*a*) for the convected vortex/hump interaction. (*b*) Fourier transform $|\bar{\tau}_w^d|$ versus the wavenumber k displays several flattened and gently sloping maxima built up by modes which are multiples of the most amplifying linear wave (cf. figure 5*b*).

surface imperfection given by (10.4) with $a = -1$. The form of an acoustic pulse remains as in (11.1) where $\delta = 0.1e/\omega$ and $\omega = 5.765$. The objective now is to further elucidate the truly nonlinear mechanism of boundary-layer receptivity, depending on whether a hump or dent of an analogous shape is placed on an otherwise flat plate. For

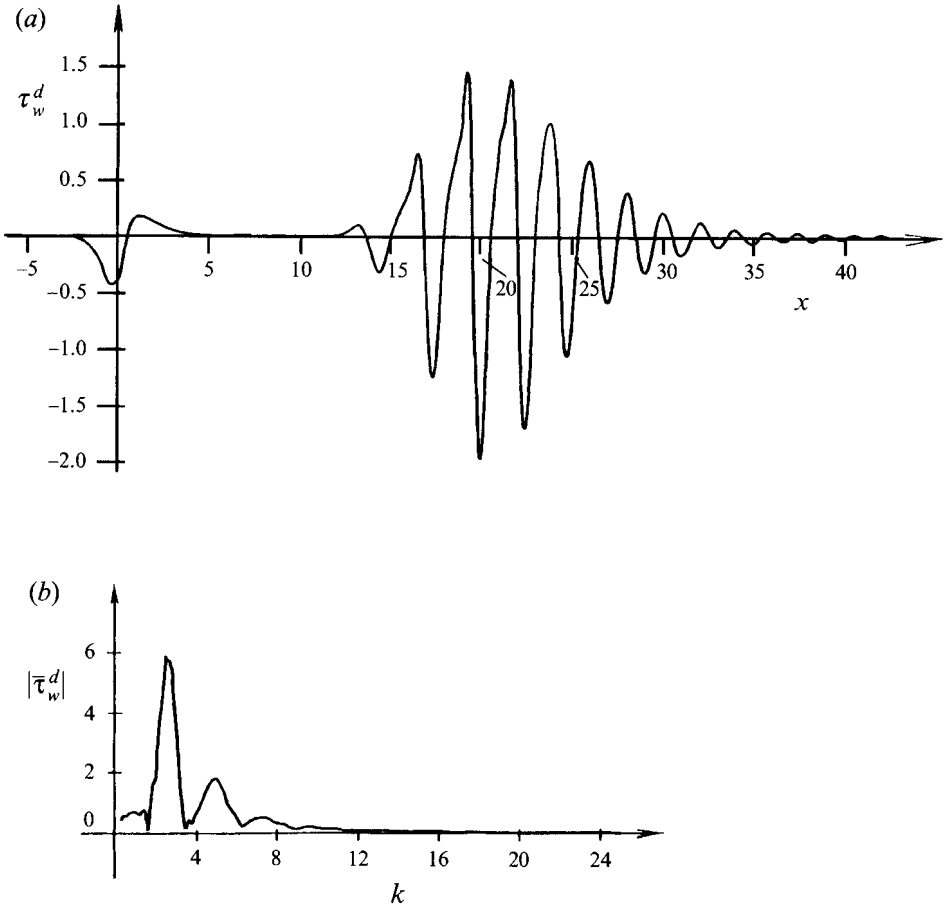

FIGURE 11. Wall shear stress and its spectrum for a wave packet generated by the sound pulse (11.1) when impinging on the dent, given in (10.4) with $a = -1$, at $t = 5$. (*a*) Distribution of τ_w^d against x demonstrates weaker oscillations than those in figure 9(*a*) provoked by a similar hump. (*b*) Fourier transform $|\bar{\tau}_w^d|$ versus the wavenumber k points out that higher-order modes just start growing.

better comparison with the previous case, the wave packet in figure 11(*a*) is again computed at the time $t = 5$. It is obvious that a dent whose depth is taken to be equal to the height of a similar hump initiates weaker disturbances, though of the same general structure. In accord with this observation, the spectrum in figure 11(*b*) contains, along with the main maximum close to $k = 2.75$, only two other local maxima built up by modes of multiplicity 2 and 3 whilst higher-order modes with $k \geqslant 10$ are almost not excited as yet. When advancing farther downstream these disturbances grow vigorously and, as figure 12(*a*) shows, detectable wiggles appear in the positive phase of one of the central cycles behind a very sharp peak in τ_w^d at $t = 5.5$ (cf. the wave packet in figure 8). In keeping with the oscillation pattern in physical space, the filling of the spectrum in figure 12(*b*) is completed over the entire interval $0 \leqslant k \leqslant 25$ of the wavenumbers. In addition to the main maximum in the vicinity of $k = 2.75$, the two subsequent maxima close to $k = 5.5$ and $k = 8.25$, which have been formed earlier at $t = 5$ (figure 11*b*), become acutely pronounced, whereas more gently sloping and flattened local maxima corresponding to modes of multiplicity 4 to 9 are formed at this later instant. Shortly after $t = 5.5$ further computations become

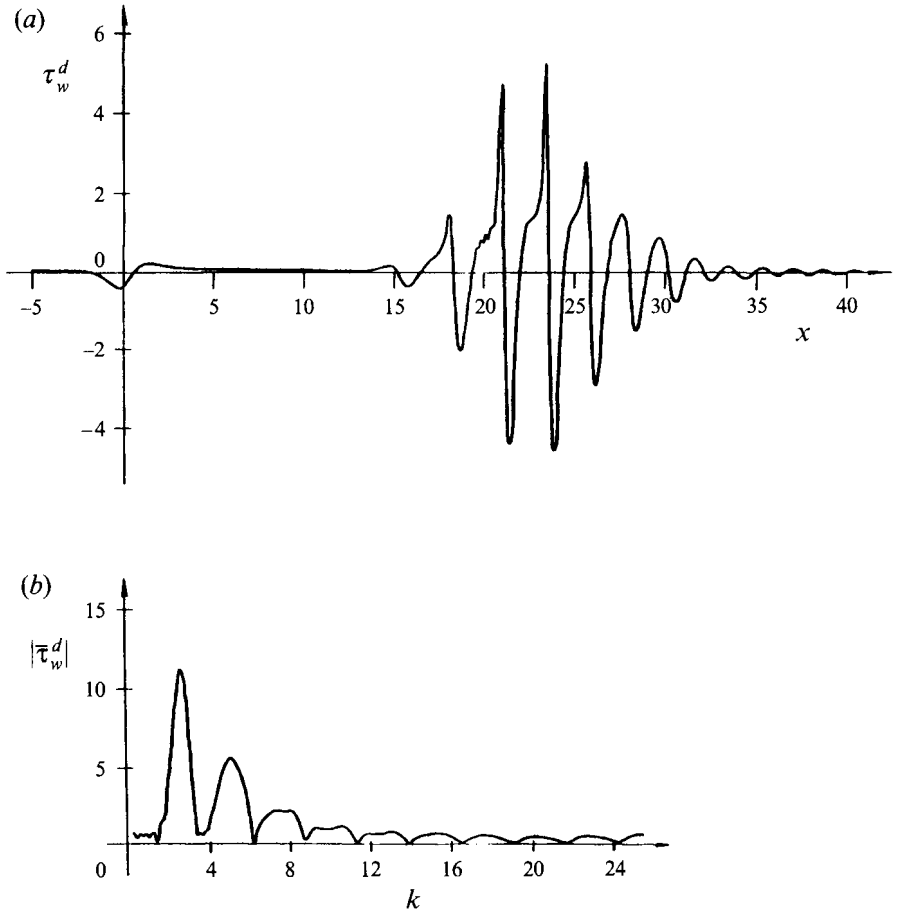

FIGURE 12. The same wave packet and its spectral content at a later instant $t = 5.5$. (*a*) Distribution of τ_w^d against x shows soliton-like negative phases within a few central cycles to be perfectly preserved whilst sharp large-amplitude spikes and short-scaled wiggles emerge in the positive phase of those cycles. (*b*) Fourier transform $|\bar{\tau}_w^d|$ versus the wavenumber k is of the almost continuous type which originates from the merging of local maxima corresponding to modes of multiplicity 2 to 9 of the fastest growing linear disturbance.

unreliable owing to excitation high-amplitude modes in distant parts of the almost continuous spectrum with local maxima being merged together.

12. Concluding remarks

Results presented above allow us to discriminate between two different regimes inherent in the potential vortex/surface-roughness interaction. The first regime may be called 'vigorous interaction', it sets in when the vortex intensity is of order 1. Theoretically, the most striking features of this type of interaction have been recognized by Walker (1978) and Doligalski & Walker (1984), then studied in Chuang & Conlisk (1989), and thoroughly investigated by Peridier *et al.* (1991*a*, *b*) using Lagrangian formulation of the problem. According to extensive computations performed by the authors cited, the high-intensity vortex filament strongly violates a boundary layer provoking a rapid lift-up of streamlines in some narrow region. An

important point is that the boundary layer starts to thicken without triggering the mechanism of viscous/inviscid interaction. At the final stage the process terminates in a separation phenomenon taking on the form of the secondary (or even tertiary) eddy and its spike-like bursting. The works by Brotherton-Ratcliffe & Smith (1987) and Smith (1988) point to the terminal singularity structure as a generic state that might be reached by the two-dimensional boundary layer at finite time even if viscous/inviscid interaction comes eventually into operation. On the other hand, when the fractional convection rate approaches 1 the boundary-layer growth occurs more gradually and integrations are carried out to larger times without revealing separation with the secondary eddy.

This suggests that another regime comes into play which may be referred to as 'turbulence-productive interaction'. Vortices featuring the second regime are of relatively small strength, but they travel not far from the body surface in line with (2.2*a–d*), (2.3*a*, *b*) and (2.4*a–d*). As a result, the vortex-induced pressure exhibits a sharp peak (figure 3) that is capable of provoking only the passive response of a Stokes sublayer adjacent to a smooth wall. In order to match still large streamwise lengthscales of impinging disturbances to much shorter ones inherent in the Tollmien–Schlichting unstable eigenmodes, some rough elements should be included in the body contour in the shape of local humps or dents for the viscous/inviscid interaction process to be initiated. Thus, the mechanism of boundary-layer receptivity to vortical disturbances is at the heart of the regime under discussion.

Usually by receptivity of the boundary layer an essentially linear phenomenon is meant which is brought about by weak external disturbing sources. However, in the particular flow environment considered here the vortex strength is not necessarily so small that a linear approximation to the Prandtl equations might be applied. Instead, an exact formulation of the receptivity problem should be used from the very beginning, making the Tollmien–Schlichting eigenmode generation change into a nonlinear process. In this case the wave packet acquires a fairly developed shape when it is still inextricably entwined with steady disturbances of the viscous wall sublayer centred around a surface roughness (figure 5*a*). For this reason, the ensuing evolution of the localized disturbances soon terminates in a violent breakdown featured by extremely sharp peaks and wiggles in the positive phases of several central cycles (figures 8 and 12*a*). Owing to an almost continuous excitation of distant parts in the Fourier decomposition of the modulated signal (figures 6*b*, 7*b*, 10*b* and 12*b*), this points to formation of an incipient turbulent spot in compliance with experimental observations by Gaster & Grant (1975), Gaster (1980, 1981), Breuer & Landahl (1990), and Cohen *et al.* (1991). Thus, the terminal stage of the wave-packet development is characterized by the progressively increasing filling of the spectrum resulting in a blow-up of the well-organized disturbance pattern. On the other hand, closed separation bubbles with recirculating fluid which are located, according to computations by Ryzhov & Savenkov (1989, 1991) and Smith (1991), within the negative phases of central cycles appear to be stable and not amenable to distortion by short-scaled oscillations in the streamwise direction.

Insofar as the wave-packet emission happens in the course of convected vortex/surface-roughness interaction and therefore is localized in time and space, there are distinct differences between a typical signal of this kind and a harmonic wavetrain (we confine our discussion to two-dimensional disturbances only). At the nonlinear stage of initially monochromatic oscillations, discrete modes of successively increasing multiplicity, in reference to the basic frequency, originate and then start amplifying. The distortion of the symmetric shape of each pulsation cycle brings about the

formation of the Benjamin–Ono algebraic solitons (Ryzhov 1990), conclusively identified in low-turbulence wind-tunnel tests with the so-called *K*-regime of transition by Borodulin & Kachanov (1988). All the pertinent data have been analysed from both theoretical and experimental sides in Kachanov *et al.* (1993). The growth of the wave-packet amplitude is accompanied by the occurrence of local maxima rather than discrete lines in the wavenumber spectrum, however, these maxima are gently sloping, flattened, and their wings overlap and actually merge together owing to disturbance modulation even at the earlier linear stage of propagation. Merging of local maxima gives rise to a continuous spectrum and explosive breakdown of the wave-packet regular structure. Continuous excitation of modes with $k \gg 1$ is a mechanism underlying the final blow-up that completely destroys the positive phases of central cycles while keeping intact their negative phases with closed bubbles of reversed flow. So, this mechanism is quite dissimilar to the abrupt focusing of the boundary layer into a narrow erupting band at the terminal stage of the separation phenomenon caused by a strong convected vortex (Walker 1978; Doligalski & Walker 1984; Chuang & Conlisk 1989; Peridier *et al.* 1991*a*, *b*).

Repercussions of the remarks set forth above for discriminating between 'natural' and 'bypass' routes to transition are crucial. The matter is that in most experimental set-ups different sources are employed to artificially excite harmonic wavetrains for measuring characteristics of the Tollmien–Schlichting eigenmodes. Data of wind-tunnel tests provide information for predicting the onset of turbulent pulsations in a boundary layer on the body surface. This forms the basis for a so-called e^n-method, well-known in practical aerodynamics (see, for example, Reshotko 1976). Predictions in the framework of the e^n-method appear to be broadly reliable as applied to aircraft wings and fuselage because nearly periodic oscillations contribute the bulk of disturbances in flight. However, if real environmental disturbances consist to a large extent of gusts, vortices, turbulent patches, and other short-scaled inhomogeneities the resulting Tollmien–Schlichting eigenmodes emerge in the form of wave packets rather than wavetrains. As elucidated in the foregoing using computational findings, the explosive nature of modulated signals is completely dissimilar to the gradual evolution of harmonic oscillations. For this reason, all of the data aimed at predicting the onset of transition should be obtained from wind-tunnel tests with wave packets artificially introduced into a boundary layer and turned to incipient turbulent spots upon blowing up (Gaster & Grant 1975; Gaster 1980, 1981; Breuer & Haritonidis 1990; Breuer & Landahl 1990; Cohen *et al.* 1991).

In connection with the turbulent spot incipience another role played by solitons merits notice. As shown by Zhuk & Ryzhov (1982) and Smith & Burggraf (1985) nonlinear travelling waves obey the Benjamin–Ono integro-differential equation provided that their amplitude exceeds the limit adopted in the present study following the triple-deck description. Just for this reason soliton properties manifest themselves within several cycles of a wave packet at the final stage before its regular pattern breaks down (figures 6*a*, 7*a*, 8, 10*a* and 12*a*). To simplify analysis, let us consider a related problem on the boundary layer adjacent to a heated plate placed vertically into a quiescent fluid in the gravity field; then the Korteweg–de Vries equation of classical mathematical physics comes into operation (Smith & Burggraf 1985). With an external disturbing agency taken into account, the equation includes a time/coordinate-dependent term on the right-hand side. Striking conclusions may be drawn from a study of periodic travelling waves where the dynamical systems theory is directly applicable (Ryzhov 1991; Burov & Ryzhov 1992). The Hamiltonian formulation reduces the problem to forced oscillations of a pendulum with quadratic stiffness and

no friction. If there is no forcing, phase-plane techniques point to the existence of an alpha-shaped separatrix loop enclosing a nested family of periodic orbits. The separatrix is an image of the Korteweg–de Vries solitons in the phase space, whereas the periodic orbits represent the travelling-wave solutions with various amplitudes. No matter how small the strength of the external source is, two (stable and unstable) manifolds appear in the phase space with an ensuing homoclinic tangle in the so-called Poincaré map in place of the separatrix loop. According to a standard procedure (see e.g. Guckenheimer & Holmes 1983), the Melnikov function can be used to give proof for trajectories with unpredictable behaviour to arise here. Vanishing of the Melnikov function along an unperturbed periodic orbit where the frequency is rationally commensurate with the forcing frequency, that is, the subharmonic orbit, reveals a subharmonic resonance. In turn, homoclinic tangles close to periodic orbits lead to random oscillations within a subharmonic resonance band. Thus, the role played by solitons and periodic large-amplitude travelling waves is twofold: they form well-organized large structures in a shear flow and, at the same time, provoke chaotic pulsations. Both properties of the nonlinear phenomenon are inseparable, implying that random oscillations spring up against a background of perfectly ordered signals. This is not the onset of real turbulence; however, flow randomization starts at the soliton stage which comes very early in the convected vortex/surface-roughness interaction process.

The last comment is due now concerning the relevance which this process may have to environments with high levels of external turbulence. Conditions for intensive free-stream turbulence to occur are observed in gas turbine engines where vortical endwall flows trailing each blade impinge against the downstream row of blades, unlike the conditions for aircraft wings and fuselage. Ensemble-averaged measurements in compressor and turbine rigs show values for turbulence levels of about 5–10% except for the wakes where values of 15–20% are registered (see, for example, Mayle 1991). Therefore, it appears that the onset of transition in gas turbine engines is first of all controlled by free-stream turbulence. Under these circumstances, transition in a boundary layer on compressor and turbine blades was found to occur in the form of a bypass mode rather than by taking the natural route peculiar to mild periodic excitation. According to Morkovin (1969), the bypass mode triggered by fairly large external disturbances does not involve the Tollmien–Schlichting stage at all. On the other hand, Walker & Gostelow (1990) have detected oscillations in the Tollmien–Schlichting frequency range travelling in a decelerated flow with a fairly low amount of free-stream turbulence. The same effect has been revealed by Kozlov (private communication 1990) in experiments with artificially excited Tollmien–Schlichting waves that emerged in spaces between turbulence spots in a boundary layer on a plate and gave rise to new spots. In keeping with observations mentioned the wave-packet spectral decompositions shown in figures 6(*b*), 7(*b*), 10(*b*) 11(*b*) and 12(*b*) testify that their major maxima in the wavenumber space are associated with the most amplifying Tollmien–Schlichting modes centred around $k = 2.75$. When excitation results in the birth of wave packets instead of a harmonic wavetrain the length of transition to turbulence becomes much shorter owing to the explosive nature of disturbance development. Indeed, the wave packet in figure 5(*a*) is closely coupled to steady inhomogeneities of the velocity field in the vicinity of the hump and those shown in figures 6(*a*), 7(*a*), 10(*a*) and 11(*a*) moved not far away from disturbing obstacles. Even an incipient breakdown in figures 8 and 12(*a*) also takes place a short distance downstream of the hump (this distance is well within two tenths of the reference wavelengths). That is why wave packets must be hardly observable in the

process of vortex/roughness interaction happening under conventional conditions in gas turbine engines. However, we may expect the production rate of turbulence spots to be strongly dependent on the presence and sizes of rough elements on a real blade. As a matter of fact, the ratio of the spot-production rate on a rough surface to that on a smooth surface varies from 10 to 30 for turbulence levels in the range of 1–2.5% in measurements reported by Mayle (1991). Direct tests on vortex/blade interactions have been conducted by Straus & Mayle (1992). In their set-up, the boundary layer at 0.1 blade cord experienced a slightly favourable pressure gradient and its mean-velocity profile was initially laminar. At this particular location, the velocity profiles appeared to remain laminar throughout the interaction, nevertheless the passing vortex induced a huge change in the turbulent energy at the peak of the interaction process. These data might be thought to be indicative of the possible generation of Tollmien–Schlichting eigenmodes in the form of modulated wave packets that evolve into turbulent spots shortly downstream. Certainly, further experiments are needed to make the latter conjecture more definite.

O. S. R. would like to express his sincere thanks to Professor Julian D. Cole for many discussions and encouraging comments. The calculation carried out as a substantial part of this research was performed using resources provided by the Computing Center, Russian Academy of Sciences. The study was supported by Air Force Office of Scientific Research under Grant F49620-93-1-002LDEF and National Science Foundation under Grant DMS-9404315.

REFERENCES

BODONYI, R. J., WELCH, W. J. C., DUCK, P. W. & TADJFAR, M. 1989 A numerical study of the interaction between unsteady free-stream disturbances and localized variations in surface geometry. *J. Fluid Mech.* **209**, 285–308.

BORODULIN, V. I. & KACHANOV, Y. S. 1988 Role of the mechanism of local secondary instability in *K*-breakdown of boundary layer. *Proc. Siberian Div. USSR Acad. Sci., Ser. Tech. Sci.* No. 18, 65–77 (in Russian; English translation: *Sov. J. App. Phys.* **3** (2), 70–81, 1989).

BREUER, K. S. & HARITONIDIS, J. H. 1990 The evolution of a localized disturbance in a laminar boundary layer. Part 1. Weak disturbances. *J. Fluid Mech.* **220**, 569–594.

BREUER, K. S. & LANDAHL, M. T. 1990 The evolution of a localized disturbance in a laminar boundary layer. Part 2. Strong disturbances. *J. Fluid Mech.* **220**, 595–621.

BROTHERTON-RATCLIFFE, R. V. & SMITH, F. T. 1987 Complete breakdown of an unsteady interacting boundary layer (over a surface distortion or in a liquid layer). *Mathematika* **34**, 86–100.

BURGGRAF, O. R. & DUCK, P. W. 1982 Spectral computation of triple-deck flows. In *Proc. Symp. on Numerical and Physical Aspects of Aerodynamic Flow* (ed. T. Celeci), pp. 145–158. Springer.

BUROV, A. A. & RYZHOV, O. S. 1992 The onset of stochastic pulsations at the early nonlinear stage of disturbance development in an incompressible near-wall jet. *Prikl. Math. Mech.* **56**, 1016–1022 (in Russian; English translation: *PMM USSR*, **56**, 921–927, 1992).

CARADONNA, F. X., STRAWN, R. C. & BRIDGEMAN, J. O. 1988 An experimental and computational study of rotor–vortex interactions. *Vertica*, **12**, 315–327.

CEBECI, T. 1979 The laminar boundary layer on a circular cylinder started impulsively from rest. *J. Comput. Phys.* **31**, 153–172.

CHUANG, F. S. & CONLISK, A. T. 1989 Effect of interaction on the boundary layer induced by a convected rectilinear vortex. *J. Fluid Mech.* **200**, 337–365.

COHEN, J., BREUER, K. S. & HARITONIDIS, J. H. 1991 On the evolution of a wave packet in a laminar boundary layer. *J. Fluid Mech.* **225**, 575–606.

COLLINS, W. M. & DENNIS, S. C. R. 1973 Flow past an impulsively started circular cylinder. *J. Fluid Mech.* **60**, 105–127.

COWLEY, S. J. 1983 Computer extension and analytic continuation of Blasius expansion for impulsive flow past a circular cylinder. *J. Fluid Mech.* **135**, 389–405.

DOLIGALSKI, T. L. & WALKER, J. D. A. 1984 Boundary layer induced by a convected two-dimensional vortex. *J. Fluid Mech.* **139**, 1–28.

DUCK, P. W. 1985 Laminar flow over unsteady humps: the formation of waves. *J. Fluid Mech.* **160**, 465–498.

DUCK, P. W. 1987 Unsteady triple-deck flows leading to instabilities. In *Proc. IUTAM Symp. on Boundary Layer Separation* (ed. F. T. Smith & S. N. Brown), pp. 297–312. Springer.

DUCK, P. W. 1988 The effect of small surface perturbations on the pulsatile boundary layer on a semi-infinite flat plate. *J. Fluid Mech.* **197**, 259–293.

GASTER, M. 1975 A theoretical model for the development of a wave packet in a laminar boundary layer. *Proc. R. Soc. Lond.* A **347**, 271–289.

GASTER, M. 1980 On wave packets in laminar boundary layers. In *Proc. IUTAM Symp. on Laminar–Turbulent Transition* (ed. R. Eppler & H. Fasel), pp. 14–16. Springer.

GASTER, M. 1981 On transition to turbulence in boundary layers. In *Proc. Symp. on Transition and Turbulence, University of Wisconsin-Madison*, pp. 95–112. Academic.

GASTER, M. & GRANT, I. 1975 An experimental investigation of the formation and development of a wave packet in a laminar boundary layer. *Proc. R. Soc. Lond.* A **347**, 253–269.

GOLDSTEIN, M. E. 1985 Scattering of acoustic waves into Tollmien–Schlichting waves by small streamwise variations in surface geometry. *J. Fluid Mech.* **154**, 509–529.

GOLDSTEIN, M. E. & HULTGREN, L. S. 1987 A note on the generation of Tollmien–Schlichting waves by sudden surface-curvature change. *J. Fluid Mech.* **181**, 519–525.

GOLDSTEIN, M. E. & HULTGREN, L. S. 1989 Boundary-layer receptivity to long-wave free-stream disturbances. *Ann. Rev. Fluid Mech.* **21**, 137–166.

GOLDSTEIN, M. E., LEIB, S. J. & COWLEY, S. J. 1992 Distortion of a flat-plate boundary layer by free-stream vorticity normal to the plate. *J. Fluid Mech.* **237**, 231–260.

GUCKHENHEIMER, J. & HOLMES, P. J. 1983 *Nonlinear Oscillations, Dynamical Systems, and Bifurcations of Vector Fields*. Springer.

HEINRICH, R. A. E. & KERSCHEN, E. J. 1989 Leading-edge boundary layer receptivity to various free-stream disturbance structure. *Z. angew. Math. Mech.* **69**, 526–598.

HARVEY, J. K. & PERRY, F. J. 1971 Flowfield produced by trailing vortices in the vicinity of the ground. *AIAA J.* **9**, 1659–1660.

KACHANOV, Y. S., RYZHOV, O. S. & SMITH, F. T. 1993 Formation of solitons in transitional boundary layers: theory and experiment. *J. Fluid Mech.* **251**, 273–297.

KERSCHEN, E. 1989 Boundary layer receptivity. *AIAA Paper* 89–1109.

KOZLOV, V. V. & RYZHOV, O. S. 1990 Receptivity of boundary layers: asymptotic theory and experiment. *Proc. R. Soc. Lond.* A **429**, 341–373.

MCCROSKEY, W. J. 1982 Unsteady airfoils. *Ann. Rev. Fluid Mech.* **14**, 285–311.

MAYLE, R. E. 1991 The role of laminar–turbulent transition in gas turbine engines. *Trans. ASME J. Turbomachinery* **113**, 509–537.

MESSITER, A. F. 1970 Boundary-layer flow near the trailing edge of a flat plate. *SIAM J. Appl. Maths* **18**, 241–257.

MILNE-THOMSON, L. M. 1962 *Theoretical Hydrodynamics*. Macmillan.

MORKOVIN, M. V. 1969 On the many faces of transition. In *Viscous Drag Reduction* (ed. C. S. Wells), pp. 1–31. Plenum.

NEILAND, V. YA. 1969 Contribution to the theory of separation of a laminar boundary layer in a supersonic stream. *Izv. Akad. Nauk SSSR, Mekh. Zhid. i Gaza* No. 4, 53–57 (in Russian; English translation: *Fluid Dyn.* No. 4, 33–35, 1972).

PERIDIER, V. J., SMITH, F. T. & WALKER, J. D. A. 1991*a* Vortex-induced boundary-layer separation. Part 1. The unsteady limit problem $Re \to \infty$. *J. Fluid Mech.* **232**, 99–131.

PERIDIER, V. J., SMITH, F. T. & WALKER, J. D. A. 1991*b* Vortex-induced boundary-layer separation. Part 2. Unsteady interacting boundary-layer theory. *J. Fluid Mech.* **232**, 133–165.

RESHOTKO, E. 1976 Boundary-layer stability and transition. *Ann. Rev. Fluid Mech.* **8**, 311–349.

RUBAN, A. I. 1984 On the generation of Tollmien–Schlichting waves by sound. *Izv. Akad. Nauk*

SSSR, Mekh. Zhid. i Gaza No. 5, 44–52 (in Russian; English translation: *Fluid Dyn.* **19**, 709–716, 1985).

RYZHOV, O. S. 1989 Boundary value problems of the asymptotic theory of hydrodynamic stability. *Proc. Steklov Inst. Maths* **186**, 124–131 (in Russian; English translation: *Proc. Steklov Inst. Maths* Issue 1, 143–151, 1991).

RYZHOV, O. S. 1990 The formation of well ordered structures from unstable oscillations in the boundary layer. *Zh. vychisl. Mat. mat. Fiz.* **30**, 1804–1814 (in Russian; English translation: *USSR Comput. Math Maths Phys*, **30**, No. 6, 146–154, 1990).

RYZHOV, O. S. 1991 Boundary-layer stability and paths to transition: theoretical concepts and experimental evidence. Invited Lecture, *1st European Conference on Fluid Mechanics*, Cambridge, UK.

RYZHOV, O. S. 1993 An asymptotic approach to separation and stability problems of a transonic boundary layer. In *Transonic Aerodynamics: Problems in Asymptotic Theory* (ed. L. P. Cook), pp. 29–53. SIAM.

RYZHOV, O. S. & SAVENKOV, I. V. 1987 Asymptotic theory of a wave packet in a boundary layer on a plate. *Prikl. Math. Mech.* **51**, 820–828 (in Russian; English translation: *PMM USSR* **51**, 644–651, 1987).

RYZHOV, O. S. & SAVENKOV, I. V. 1989 Asymptotic approach in the hydrodynamic stability theory. *Math. Modelling*, **1** (4), 61–86 (in Russian).

RYZHOV, O. S. & SAVENKOV, I. V. 1991 On the nonlinear stage of perturbation growth in boundary layer. In *Modern Problems in Computational Aerodynamics* (ed. A. A. Dorodnicyn & P. I. Chushkin), pp. 81–92. CRC Press.

RYZHOV, O. S. & TERENT'EV, E. D. 1984 Some properties of vortex spots in a boundary layer on a plate. *Dokl. Akad. Nauk SSSR* **276**, 571–575 (in Russian; English translation: *Sov. Phys. Dokl.* **29** (5), 349–351, 1984).

RYZHOV, O. S. & TERENT'EV, E. D. 1986 On the transition mode characterizing the triggering of a vibrator in the subsonic boundary layer on a plate. *Prikl. Math. Mech.* **50**, 974–986 (in Russian; English translation: *PMM USSR* **50**, 753–762, 1986).

SMITH, C. R., WALKER, J. D. A., HAIDARI, A. H. & SOBRUN, U. 1991 On the dynamics of near-wall turbulence. *Phil. Trans. R. Soc. Lond.* A **336**, 131–175.

SMITH, F. T. 1988 Finite-time breakup can occur in any unsteady interacting boundary layer. *Mathematika* **35**, 256–273.

SMITH, F. T. 1991 Steady and unsteady 3-D interactive boundary layers. *Comput. Fluids* **20**, 243–268.

SMITH, F. T. & BODONYI, R. J. 1985 On short-scale inviscid instabilities in flow past surface-mounted obstacles and other non-parallel motions. *Aero. J. R. Aero. Soc.* **36**, 205–212.

SMITH, F. T. & BURGGRAF, O. R. 1985 On the development of large-sized short-scaled disturbances in boundary layers. *Proc. R. Soc. Lond.* A **399**, 25–55.

STEWARTSON, K. 1969 On the flow near the trailing edge of a flat plate II. *Mathematika* **16**, 106–121.

STEWARTSON, K. & WILLIAMS, P. G. 1969 Self-induced separation. *Proc. R. Soc. Lond.* A **312**, 181–206.

STRAUS, J. & MAYLE, R. E. 1992 Boundary-layer measurements during a parallel blade–vortex interaction. *AIAA Paper* 92–262.

TUTTY, O. R. & COWLEY, S. J. 1986 On the stability and numerical solution of the unsteady interactive boundary-layer equation. *J. Fluid Mech.* **168**, 431–456.

VAN DOMMELEN, L. L. & SHEN, S. F. 1980 The spontaneous generation of the singularity in a separating boundary layer. *J. Comput. Phys.* **38**, 125–140.

VAN DOMMELEN, L. L. & SHEN, S. F. 1982 The genesis of separation. In *Proc. Symp. on Numerical and Physical Aspects of Aerodynamic Flow* (ed. T. Cebeci), pp. 283–311. Springer.

WALKER, G. J. & GOSTELOW, J. P. 1990 Effects of adverse pressure gradients on the nature and length of boundary layer transition. *Trans. ASME J. Turbomachinery* **112**, 196–205.

WALKER, J. D. A. 1978 The boundary layer due to rectilinear vortex. *Proc. R. Soc. Lond.* A **359**, 167–188.

WILLIAMS, J. C. 1977 Incompressible boundary-layer separation. *Ann. Rev. Fluid Mech.* **9**, 113–144.

ZHUK, V. I. & RYZHOV, O. S. 1982 Locally nonviscous perturbations in a boundary layer with self-

induced pressure. *Dokl. Akad. Nauk SSSR* **263**, 56–59 (in Russian; English translation: *Sov. Phys. Dokl.* **27** (3), 177–179, 1982).

ZHUK, V. I. & RYZHOV, O. S. 1983 Asymptotic behaviour of solutions of the Orr–Sommerfeld equation that yield unstable oscillations at large Reynolds numbers. *Dokl. Akad. Nauk SSSR* **268**, 1328–1332 (in Russian; English translation: *Sov. Phys. Dokl.* **28** (2), 87–89, 1983).